ISABEL MOREIRA DE OLIVEIRA

# Development of a new connection system for reticulated shell structures using parametric modeling and digital fabrication

São Paulo

2019

**ISABEL MOREIRA DE OLIVEIRA**

# Development of a new connection system for reticulated shell structures using parametric modeling and digital fabrication

**Original Version**

Master Thesis presented to Escola Politécnica da Universidade de São Paulo to obtain the degree of Masters in Science in Civil Engineering

Concentration area:

Structural Engineering

Advisor:

Prof. Dr. Ruy Marcelo de Oliveira Pauletti

São Paulo

2019

Catalogação-na-publicação

**RESUMO**

Estruturas leves em forma de grade formadas por elementos de barra unidos por nós são chamadas de estruturas reticuladas, ou *gridshells*. Diferentes sistemas estruturais são estudados, e um novo sistema estrutural e método de geração deste sistema são propostos. O sistema de conexão pode ser usado em estruturas de superfícies de curvaturas e parâmetros de conexão variáveis. Antes do desenvolvimento deste sistema, as escolhas de materiais, tipos existentes de conexões, padrões da grade, sistemas de revestimento, métodos de otimização e avaliação de análise estrutural são apresentados. Cada aspecto enumerado permite o desenvolvimento bem fundado do sistema de conexão. A conexão desenvolvida utiliza um perfil padronizado, chamado de *hub*, e peças conectoras. As barras da estrutura se unem aos hubs através destas peças conectoras, que absorver parâmetros variados da conexão, como ângulo de incidência, ângulo de torção, ângulos de adjacência, e tolerância de fabricação de tamanhos das barras e conexões aparafusadas. A meta é produzir um sistema que possa ser rapidamente montado, desmontado e reutilizado. Um ambiente paramétrico de modelagem é utilizado para modelar geometrias globais e locais de malhas e nós. Dados de entrada da definição paramétrica inclui uma malha, geometria das ranhuras do hub, e seção transversal das barras; dados de saída inclui tamanho das barras, geometrias das peças conectoras, e informação de construção. Uma análise de estabilidade estruturas é conduzida com software paramétrico de elementos finitos. Um modelo físico é apresentado, servindo de validação do conceito desenvolvido no ambiente de modelagem computacional. A escalabilidade do modelo é discutida, sendo levada como ponto de partida a experiencia da produção do modelo de pequena escala. Os resultados dos ensaios de tração do material e da conexão são fornecidos.

Palavras-Chave: Sistema de conexão. Estrutura reticulada. Grid shell. Gridshell. Programação paramétrica.

**ABSTRACT**

Lightweight structures in grid form made of bar elements joined together with nodes are called reticulated shells, or gridshells. Different gridshell structural systems are studied, and a new connection system and method for generating this system are proposed. The connection system applies to structures with surfaces that have a high variability of curvature and connection parameters. Prior to the development of such a connection, the choices of materials, existing types of connections, grid patterns, cladding systems, optimization methods, and structural analysis evaluation are presented. Each enumerated aspect enables a well-reasoned development of the connection. The connection uses standardized hub geometries and interconnecting parts. The bars of the structure connect to the hubs through these interconnecting parts, which absorb varying parameters of the connection, such as incidence angle, twist angle, adjacency angles, and the fabrication tolerance of bar lengths and bolted connections. The aim is to provide a system that can be assembled quickly, disassembled and reused. A parametric modeling environment is used to model global and local geometry of meshes and nodes. Inputs for the programmed parametric definition include a mesh, geometry of the hub notch, and bars cross-sections; outputs include bar lengths, interconnecting parts geometries, and assembly information. A structural stability analysis is conducted with parametric finite element software. A small-scale physical model is presented, serving as a proof of the concept developed within the computational modeling environment. The scalability of the model is discussed, taking as a starting point the experience of the production of the small-scale model. Tensile tests results of the printed material and connection are provided.


Keywords: Connection system. Joint. Reticulated shell. Grid shell. Gridshell. Parametric programming.

# CONTENTS

# AGRADECIMENTOS

Agradeço, primeiramente, ao meu orientador, professor Ruy Pauletti, por valorizar a criatividade, pelas discussões filosóficas de estruturas futurísticas, pela sua visão crítica, procurando questionar o porquê de cada escolha em um projeto, e por me apresentar diferentes temas e incentivar participação em diversos projetos.

À professora Leila Meneghetti, agradeço por toda a atenção ao longo desta jornada, por oferecer sua orientação em diversas etapas do projeto, e por ser um forte exemplo feminino na nossa área de atuação. Considero-a minha coorientadora.

To professor Sigrid Adriaenssens, I thank the invitation for the one month stay at Princeton.

Aos meus pais, agradeço o apoio incondicional à busca do conhecimento e felicidade, e por não medirem esforços para que eu tivesse as ferramentas necessárias para realizar esta pesquisa.

Agradeço aos meus tios Wanda e Mário pelo acolhimento em São Paulo, e aos primos e primas de São Paulo que proporcionaram tantos momentos bons ao longo destes anos. Agradeço também à família do Rio, que me acompanhou neste caminho, sempre curiosa com o projeto que estava em desenvolvimento e preocupada com minha adaptação à cidade.

Aos novos amigos de São Paulo, agradeço enormemente pela companhia, conversas e abertura desde o início. Ao Gustavo, agradeço por compartilhar tantos dos seus amigos comigo, e pela sua amizade desde o primeiro dia de aulas. À Yasmin, agradeço por ser meu porto seguro ao longo desses anos, e por ser minha maior companhia de cafés da manhã.

Aos amigos do Rio de Janeiro, agradeço por se manterem sempre presentes, com eventuais visitas e me acompanhando à distância.

Agradeço à secretaria do programa pela gentileza e pela ajuda com os processos internos. Agradeço também aos grupos do LMC e da Asteróide pela companhia, e à Debora e à Júlia por concordarem em montar o modelo físico apresentado nesta dissertação. Agradeço ao professor Arthur, Fernando e Thiago pelas discussões sobre diversos projetos e arquitetura paramétrica, e por estarem sempre dispostos a colaborar.

# 1 Introduction

Reticulated metallic structures, or gridshells, have been around since the beginning of the 1900s (Geometrica n.d.). These lightweight structures consist mainly of bars and nodes, and they can cover long spans. In aerospace engineering history, the reticulated structures have been used to construct airplanes (RAF 1943), and in civil construction, they can be applied to the building of roofs (Schober 2015) and façades (Asymptote 2010). Historically, reticulated structures relied heavily on standardized elements, and only certain types of forms could be built. However, the forms of such structures grew in complexity over time (Charest et al. 2019). The number of types of connections for gridshells has continuously increased, as well as the need for their versatility of uses and applications.

Additive manufacturing (3D printing)[1] was very restrictive until late 2010 (3DPrintingIndustry 2017; Goldberg 2018). 3D printing was popularized over the years and is now more accessible. It becomes attractive to use these innovative practices to further develop the reticulated structures, given that they apply to many purposes, and that new fabrication techniques are available at lower costs.

Parametric programs, linked to structural and optimization tools, allows analyses of much more complex forms and practical exploration of structures in early design stages. The parametric programs allow exploration and creation of new tools for future design demands. Although no single parametric method fits all projects, flexible and customizable programs may be useful to a wide range of structures. Thus, there must be an evaluation of key input parameters, and for that, it is imperative to have a comprehensive background of the gridshell structures and how these structures may vary. Some background on these structures include form-finding of the structure; multilayer properties of such forms; the materials commonly used for these structures; the existing connection systems; the boundary conditions; and optimization methods for further improvements in the construction of lighter and more resistant structures. This extensive background is used to develop a connection system for

---

[1] Additive manufacturing has a broader definition than 3D printing (Labonnote et al. 2016); however, for the purposes of this work they will be addressed in the same manner.

rigid gridshells. The connection system is programmed in a parametric environment, where input parameters automatically change the geometry of the connection elements.

A significant volume of work of gridshells on site is due to the number of connections. Thus, the number of unique connections and elements should not change that volume of work considerably, provided there are trained workers, or that the construction method is simple enough.

As the scalability and feasibility of the connection system are both concerns, standardized hubs can be used to reduce the volume of printed material. Additionally, reduction of the geometry minimum bounding box[2] is essential since most high precision additive manufacturing techniques are still very time consuming and limited to the size of the machine available. Although high precision metal printing robotic arms with movable bases are a reality ("MX3D" n.d.), they are still uncommon. Reducing the volume of material destined to form the unique elements of the structure is also intended to reduce production cost and waste. Although this is a subjective matter, for it depends on location and popularization of such machines over time, higher strength materials and higher product quality tend to be more expensive.

The production of gridshells using additive manufacturing is an area in expansion and demands additional studies. A crescent number of projects use additive manufacturing to provide solutions for connection systems of complex gridshells with entirely 3D printed nodes (or printed molds for casting) (Seifi et al. 2018; Kassabian, Cranston, and Lee 2017; N. Williams et al. 2015; Hassani et al. 2019). However, the use of standardized hubs in combination with 3D printed interconnecting pieces have not been found in the English literature to provide a solution for gridshell connection systems. This combination needs exploration.

In the present study, we developed a new rigid gridshell connection system with automated parametric generation of local geometry from an arbitrary globally discretized surface (or mesh). A small-scale physical model proves the concept of the connection system developed in computational environment. The proof of concept is a step before prototyping and large-scale production (Bisplinghoff 1969).

---

[2] A box with minimum measurements that encloses the entire geometry.

## 1.1   Motivation

> There is still a widespread misunderstanding concerning the role of architects and structural engineers: it is said that architects are the designers of a building from concept to detail, whereas the engineers (only) care for its stability. In fact, it is its function which clearly attributes a building to either an architect or an engineer only, or to both: to an architect only if it is multifunctional in a social context – typically a family house where no engineer is needed – and to an engineer only if it serves a singular structural purpose – typically built infrastructure such as a bridge where no architect is needed. A high-rise building typically needs both, an architect and an engineer. (…) Shells play a special, singular role for engineers. Their shape directly derives from their flow of forces, and defines their load-bearing behavior and lightness, saving material by creating local employment, their social aspect. (Schlaich 2014)

The motivation of the present study came from the will to turn projects with aesthetic quality and commonly unfeasible into projects that are viable. Varying curvatures, long spans, challenging architectural specifications are usually accompanied by high costs, the necessity of highly skilled workers, and excessive use of materials. New manufacturing techniques, development of computer software for both architectural design and engineering analysis allows for ways to improve the design, the speed of construction, the efficient use material, and so on. The quality of data visualization itself reduces possible detailing errors. As an engineer, to help bridge the gap between engineering and architecture, to care for aesthetic quality, to employ local workers, without the need of previously specialized ones, and to help save material are all a starting point for this study and development of the structural system.

## 1.2   Objective

**General objective:**

To develop a reticulated shell structural connection system with automated generation of local parametric geometry from an arbitrary globally defined surface.

**Specific objectives:**

- To create a bar-hub connection system that can be applied to gridshell projects with varying parameters
- To create a computational platform to automatically generate the connection system for different meshes in a parametric environment

- To prove the concept developed with a physical model, creating room for future development of large-scale applications

## 1.3 Structure of the Text

This text is divided into seven parts: this is the first section, a brief introduction to the context. The second is a literature review, where the most cited and relevant work are briefly introduced. The third section provides the necessary comprehensive background to the design of gridshell structures, exposing form, materials, construction methods, grid pattern definition, layers, boundary conditions, structural analysis, buckling evaluation, structural optimization in structures, and different connections for gridshells. The fourth section presents the developed structural system, the computational implementation details, the definition of global and local parameters, and the physical model project. The fifth part shows the results of this study, including the assembled physical model, the conducted tensile tests; and numerical applications. The sixth part presents discussions of the current applications of the proposed system, its scalability, and the experience of building the physical model. The conclusion is contained in the seventh part. Finally, future works are proposed.

# 2 State-of-the-art

This section presents a brief review of the state-of-the-art works used in this dissertation.

"AAD_Algorithm Aided Design" (Tedeschi 2014) explains the development of computer-aided design tools through the years. It states the main advantages of using Rhinoceros and Grasshopper and identifies many helpful software to add to the plug-in (add-ons).

"Shell structures for architecture" (Adriaenssens, Block, et al. 2014) is a book that covers a wide range of topics in shell structures, continuous or discrete. Many structural optimization methods are covered, and a wide variety of constructed projects are presented. This book references many fundamental works in diversity of light weight structures.

"Guide to Buckling Load Evaluation of Metal Reticulated Roof Structures" (Kato 2014) provides detailed studies on buckling evaluation of both single and double layer reticulated shells. This guide is a collection of best practices of the structural analysis of these structures, with a detailed evaluation of buckling loads. An objective workflow to evaluate buckling loads is presented, and as the reader advances, the complexity of the structures addressed increases.

Milos Dimčić (Dimčić 2011) approaches fundamental topics to free form gridshell design in this study. The author provides insights as to why we should study free form structures and how it relates to Nature's building process. The author also states we should sustain architects' creativity and not always reshape the surfaces so that they become optimal. Instead, we should study how to build the given structure optimizing material property, cross-section, geometry, and topology. Dimčić shows that intricate structural systems are feasible using new technology and manufacturing processes. Dimčić summarizes the formulation for Bèzier curves and how they are mathematically manipulated to compose a NURBS[3] surface. The author, then, works towards paneling a predefined surface.

Architectural Geometry (Pottmann et al. 2015) is a survey paper that presents geometric properties of structures and of structural elements, and how these properties influence structural performance. It presents polyhedral meshes, such as triangular, quadrilateral and

---

[3] "Non-uniform rational basis spline (NURBS) is a mathematical means of defining freeform surfaces defined by a set of control points, which allow a user-friendly creation and modification of shapes." (Winslow 2014)

hexagonal, pointing out their main characteristics and challenges. The authors provide a perspective on fabricating curved surfaces without the use of planar panels. They point out how panel repetition is often the key to keeping the project within budget. The authors also provide methods to make structures with torsion free connections through the correct choice of subdivision curves. Furthermore, the first author participates in a series of published works (Liu et al. 2006; Pottmann et al. 2007; Pottmann, Brell-Cokcan, and Wallner 2007; Pottman et al. 2007; Yang et al. 2011) presenting formulations for gridshell meshes, how they can be efficiently optimized for a smarter production and assembly, and how the geometries with predetermined constraints relate to aesthetic architectural forms. These publications explicit the importance of constant attention to the fabrication process in early design phases, or *fabrication aware design*.

Research by Maiola (1999) shows, with experimental analysis, why flat end bars should be avoided, although they do provide a simple solution for reticulated metallic structures. Although this work is not recent, it provides justification for the exploration of different connection systems.

The book "Transparent shells" by Hans Schober (2015) explains various aspects of projecting and building rigid gridshells (mainly) with glass cladding. It shows projects the author has built and it presents some rules of thumb to guide general structural choices, such rise to span ratio of gridshells and how this relates to structural efficiency and use of material. Most of the gridshells presented in this book have planar quadrangular grids prestressed with diagonal cables. The justification is that usually cladding material is cut out from rectangular glass sheets, thus, lowering waste of material; and that quad meshes have simpler nodes (four bars, one node) than triangular ones (six bars, one node). This book shows geometric exact forms that allow easier manufacturing maintaining aesthetic compliance. The form-finding process can be helpful to lower costs in some cases, especially those with high bending moments and challenging boundary conditions. Sometimes, though, this kind of optimization increases manufacturing difficulties and lowers costs only marginally.

A series of works published (Mesnil, Douthe, Baverel, et al. 2018; Mesnil, Douthe, and Baverel 2017; Mesnil et al. 2017; Mesnil, Douthe, Richter, et al. 2018; Tellier et al. 2018) compare the structural aspect of grid shapes optimization of grid subdivision, different cladding generated, all, in some way, focused on fabrication aware design. These publications indicate the direction

of engineering studies for lightweight structures. Grid pattern studies inform what might be the tendency of the number of bars per node, of the varying grid and surface parameters being used, etc.

A variety of works present connection systems for reticulated shells using additive manufacturing or robotically produced formwork ("Architecture+Fabrication: MakeTANK" 2018; Warton, May, and Kovacevic 2017; Kassabian, Cranston, and Lee 2017). These studies show constant evolution of structural system developments.

Finally, an article with some remarks on the construction of a gridshell was published (Gerasimov et al. 2018), providing a good example of the choices and analysis needed to construct the project. In this article, they point out the importance of the grid generation, the positioning of the supports, the critical loads, aesthetic quality, types of connecting joints required to build a safe structure, and how they optimized member cross sections to reduce material usage. The mesh was decided to be triangular, and the angle between bars are as close to 60 degrees as possible. The decisions made for this project are approached in this dissertation.
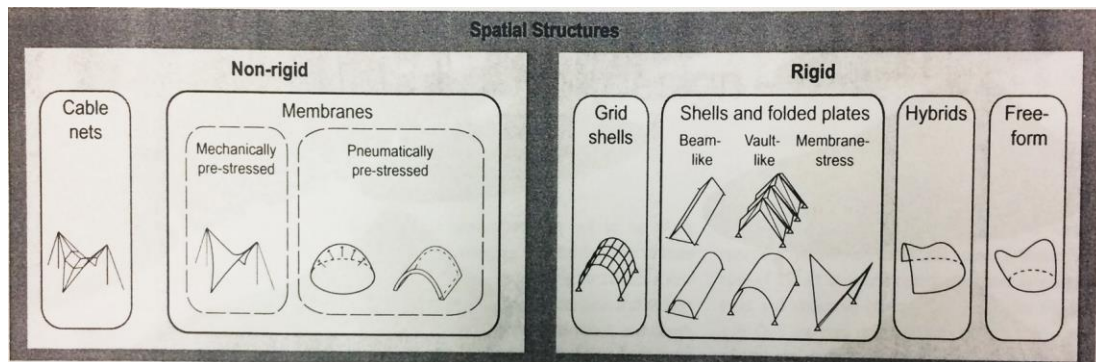
# 3 Gridshells



*Figure 1: Spatial Structures* (Bechthold 2008)

Spatial structures, or light structures, are defined as such by its much-reduced weight over the area covered. First, in (Bechthold 2008) there is a general classification of spatial structures, the author separates them in non-rigid and rigid (Figure 1). The non-rigid ones are cable nets and membranes, either mechanically or pneumatically pre-stressed. The rigid ones are grid shells, shells and folded plates, hybrids and free-form. The main difference between these two broader classifications includes the material used: if it can be submitted to compression, tension, bending, and shear forces, then the structure is rigid; if it is only tensioned, then the structure is non-rigid. Another difference is the relatively small displacements in relation to the structure's span presented by rigid structures when compared to non-rigid. According to Bechthold, the construction systems have been less dependent, over the years, on the excessive use of pattern and repetition for the structures to be economically viable. This book is from 2008, and as a matter of fact, we have been experiencing this change over the years. Perhaps if one looks closer at a structure seemingly with no repetition, one might notice some hidden pattern over most elements of the structure. Although not common, there are examples of structures with close to zero repeated elements (Menges et al. 2017).

The term gridshell is used in this dissertation to refer to any light structure that is subdivided into discrete elements and can be subjected to different types of forces, not only tension. These elements may present structural continuity from one side of the span to the other, or be visibly discrete and connected by nodal elements. In some works, the structures presenting continuous members bent in place are called elastic gridshells (Hernández, Baverel, and Gengnagel 2013), or simply gridshells. In other studies, the grid-like structures subdivided into discrete elements are called reticulated shells (Kato 2014), rigid gridshells (Bechthold 2008) or,

simply, gridshells (C. Williams 2014). These rigid gridshells are usually built with elements in their final shape, that are progressively joined together in the grid formation. This characteristic is usually chosen alongside the material of the structure. Elastic gridshells tend to be made of wood, bamboo (Figure 2a) or composite materials, such as glass fiber reinforced polymer (Figure 2b) (Tayeb et al. 2015) and recycled materials like paper (Figure 2c). Rigid gridshells are usually made of metallic materials, such as aluminum or steel (Figure 2d,f), but they are also found in timber, plywood (Figure 2f) and bamboo.

> "The terms 'gridshell', 'lattice shell' and 'reticulated shell' all mean essentially the same thing, a shell structure made of a grid, lattice or net of elements of any material, or possibly a continuous surface with lots of holes. The word 'reticulated' comes from the Latin 'reticulum', meaning a small net" (C. Williams 2014)
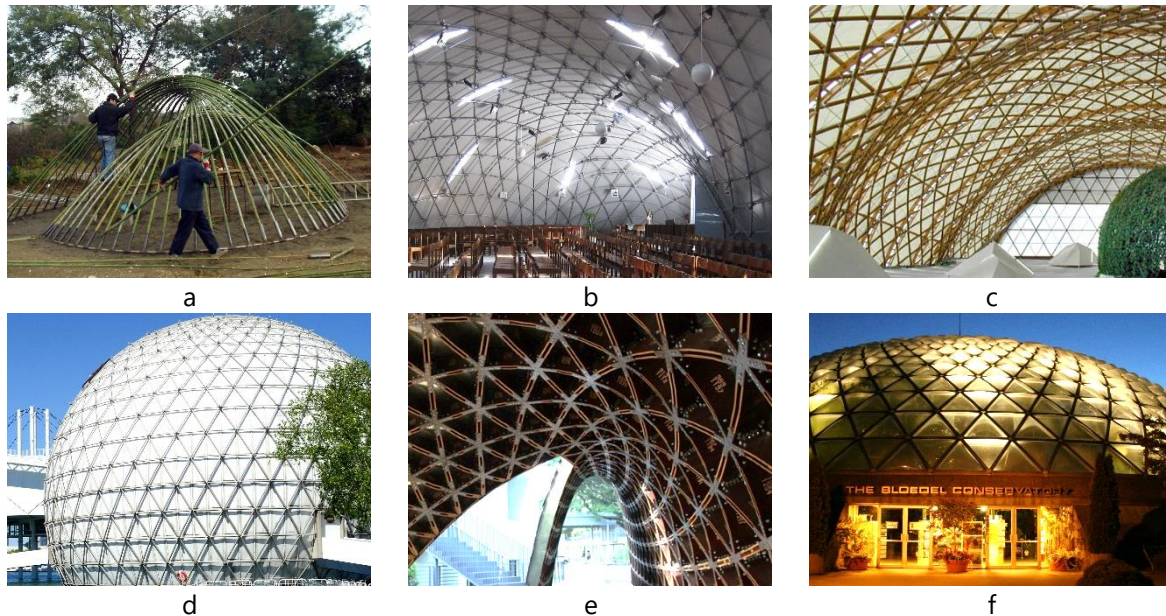


*Figure 2: Different gridshells: (a) Bamboo Structure* (Khazaeli 2009)*; (b) Gridshell of Créteil* (Lionpeloux 2013)*; (c) Japan Pavilion* (Dalbéra 2010)*; (d) Ontario Place Cinesphere; (e) SUTD Library Pavilion* (Kalvo 2013)*; (f) the Bloedel Conservatory* (Taz 2006).

Each choice to be evaluated in these structures is mentioned in this introductory part of this section and later expanded in each subsection. The separation of topics was inspired by a lecture by Chris Williams (2017).

The grid pattern in cases of elastic gridshells is usually quadrangular, with nodes that allow for very small rotations of the elements, only for the accommodation of the structure. Once the structure is in position the connections, usually bolts, are tightened to increase rigidity. The grid pattern for rigid gridshells is usually found as quadrangular or triangular. Other patterns

can also be found, such as hexagonal (Dimčić 2011) and Kagome (Mesnil, Douthe, and Baverel 2017). Non-triangular patterns require more study of the stability of the structure and of the planarity of the faces if they are to be covered with glass. Other cladding materials such as ETFE cushions and bent metallic plates are also explored for different patterns. Metallic plates can be folded such as the hexagonal meshes on (Tellier et al. 2018). For elastic gridshells, often the cladding is of flexible material like membranes (Tayeb et al. 2015); however, glass cladding can also be found in the 2007 Chiddingstone Orangery (Adriaenssens, Barnes, et al. 2014). For the latter case, the elastic gridshell was stiffened with braces and had fixed/rigid boundary conditions. Another key specification in light structures projects is the study and definition of boundary conditions; specifying relevant load cases and supports. When building curved structures, the resulting reaction forces are usually given in a diagonal in relation to the ground surface, with vertical and horizontal components. It is often the case where tension and compression rings are applied to such structures. These rings are present in many stadium designs to account for the horizontal component of the resultant, so only vertical forces are transferred to columns. In some cases, when the structure is placed close to ground level, diagonal transfer elements can be used, and a tension ring can be built under the ground level for a vertical foundation. Understanding the relations of rollers, pins or fixed supports regarding the structure's stiffness and its relation to buckling loads is also important. Rollers might lower buckling loads, and fixed ends can increase it.

The connections of the discrete members have a direct relation to the rigidity of the structure. Nodal connections can be welded, bolted, tied, or screwed in place. Each type of connection has its respective stiffness, and the way this connection is modeled is key to evaluating forces in the structure. Maximum displacements, buckling evaluation, and the relation between the cladding system and support structure can change how the sections are dimensioned. Temperature variances, for instance, may change how thermal expansion of the cladding system influence the support structure, depending on how the connection detail is generated.

Construction method stages also require stability analysis. Temporary scaffolding may be needed, the sequence of construction can directly affect how well the last elements are assembled. The quality control of the process is important, with the precision of production alongside precision of execution. The way the elements are tagged is vital, they should be almost intuitive to understand. There is technology available for large scale projects that might

be needed for higher quality complex projects and provide higher construction speed. Coded tags may be used, they can be read by cellphone or tablets to verify the location of each element on site.

The structural analysis of gridshells must also be very well thought of. Theory of gridshells is derived from continuous shells, and guidebooks contain the analytical formulations of the most commonly constructed surfaces. However, if the surface presents variances, then detailed linear and non-linear analyses must be carried out.

Each choice in a grid shell structure leads to a great variety of secondary choices and consequences that have complex relations between one another. Form, geometry, mesh pattern, layers, material, construction method, boundary conditions, connection detail, cladding type, and structural analysis technique are all mentioned in this dissertation. The variety of such characteristics is enormous, and, although there is vast material on such topics, there is also a vast number of new questions to be asked regarding new technological advances on construction methods, materials, and structural systems.

In the sequence of a project, first, it is usually the cladding of the grid shell that is chosen; it is often the case where the transparent shells are wanted (C. Williams 2017). This first decision is a principal guide for the limitation of further design specifications. The support structure of the shell is then discussed: the grid pattern, if it is a single- or multi-layer structure, the materials for the grid elements, and so forth. The geometry of the grid itself (mesh generation) needs to consider many aspects: the maximum possible size of the cladding; the material of the support structure, which defines member sizing; and boundary conditions, which may define important mesh generation lines.

These described decisions are all considering one other major step has been taken: the form of the surface in space. The forces of the cladding material, accidental forces of people on the structure, wind pressure, and depending on the location, earthquake and snow loads can be used to generate a surface that will allow for slenderer sections and, therefore, less material and cost-saving solutions. This is called form finding.

## 3.1   Form

Shells are structures that take advantage of curvature to reach larger spans without the need to increase its elements cross section as much. The shape to which the rise to span ratio becomes optimal, with respect to the governing load, has been studied for years. Physical models were an indispensable tool at first to understand the form certain shapes might take. Antoni Gaudí, Heinz Isler, and Frei Otto are largely known for these models, but others before them started developing mathematical representations and physical models as well (Addis 2014). First, Robert Hooke published in form of an anagram, and later Richard Waller published (Ochsendorf and Block 2014) that the mirrored shape to which a hanging chain assumes (catenary) is submitted only to compression. Such a shape can have a minimal cross-section without bending moments. This concept has been largely applied to problems with higher complexity. Methods that do not rely on physical modeling were developed, and are largely used for different load cases and for more complex initial forms.

Two form-finding methods are the force density (Linkwitz 2014) and the dynamic relaxation (Adriaenssens, Barnes, et al. 2014). Both approaches have been implemented in software add-ons. Other methods have also been developed (Jiang et al. 2018; Richardson et al. 2013).

Gridshell forms are usually optimized to gravity loads, as they tend to be the governing load on many occasions; it is, after all, the load to which the structure will be subjected to most of its life span. For earthquake-prone areas, other formulations have been included to account for such loading.

In Schober (2015) it is possible to take notes on characteristic values for common rise to span ratios that are optimal for rigid gridshells with glass cladding. Spherical domes, for instance, should present a ratio between 0.14 and 0.50.

## 3.2   Materials and Construction Methods

Materials for the grid components, as mentioned before, can be wood/timber, aluminum, steel, or composites. Cladding components are usually glass, but can also be membrane, steel plates, ETFE cushions, or other types of paneling. For each type of material there is usually a corresponding construction method closely related to the connection type.

It is common to build from the borders to the inside for reticulated structures with expressive curvature. Scaffolding is required to reach higher elevations for most types of structural systems, and materials may be lifted with cranes. For others types it is impressive how almost only cranes are needed; both the practicality of the construction method and the employment of skilled workers are crucial (Geometrica n.d.).

Elastic gridshells are made from materials with elastic bending properties. One known construction method is described following. Rails are installed on the ground level. Then the straight elements are placed in a form of a grid on the ground, edges aligned to the rails, and then the nodes are installed. The edge vertices are pined to the rails and pushed towards the center of the geometry. The central highest vertices can be lifted by a crane. When elements are in the final bent position, then the nodes are tightened so in-plane rotation is completely locked.

## 3.3    Grid pattern definition, layers, and boundary conditions

Gridshells can have a single layer, two layers, or more, although structures with more layers are quite unusual. Some characteristics of each type are listed below:

- Single layer
    - Practically no depth to install equipment
    - Quite flexible in terms of out-of-surface bending behavior
    - Prone to shell-like buckling
    - Usually rigid or semi-rigid connections are adopted and modeled
    - Aesthetically pleasing, slender outline
- Double and multi-layer
    - Provide room to install equipment
    - Combined action between upper and lower chords with web members provide large bending stiffness
    - In most cases, the buckling pattern appears as member buckling. Almost no displacements at nodes but buckled members show large rotations at nodes.
    - Usually pin-connections are adopted when modeling, although real connections are semi-rigid. (Kato 2014)

        o    More material is used, but wider spans can be reached

Regarding support conditions, Figure 3a shows a dome with a tension ring around the border so only vertical loads are transferred to the vertical columns. It can be quite dull compared to Figure 3b nevertheless, with distributed buttresses around its perimeter to properly transfer the load to the foundation. These diagonal members may, then, transfer horizontal loads to a tension ring under the ground level. Specifically, a structure (Palazzetto dello Sport in Rome) with this concept appears in (Schlaich 2014) as an example of a support structure proposed by creative engineer Pier Luigi Nervi. The mentioned structure has Y shaped buttresses, and it is aesthetically more pleasing than the simplified image created here.



a                                b
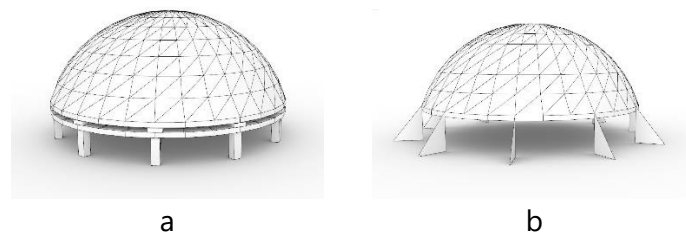
*Figure 3: Support structures: (a) tension ring and vertical columns; (b) diagonal members used for load transfer.*

Each type of polygonal mesh has its positive and negative remarks, and most of the work produced in this dissertation is focused on triangular meshes. Following is presented a set of characteristics for both.

Triangular and quadrangular grids are often seen in gridshell projects, but other grid shapes can be generated, such as hexagonal grids. Less used grid shapes require further study on every structural member connectivity, planarity, and sizing of panels. The Kagome (Mesnil et al. 2017) gridshell is shown to be structurally more efficient than an unbraced quadrangular mesh, however, it is not as commonly used. Furthermore, quadrangular meshes are typically braced diagonally (Figure 4a,b): cables are installed forming crosses on the quadrangles, they act in tension, and they increase the in-plane shear stiffness. These members can also be pretensioned. The braces can increase buckling load in single layer domes, and they are more useful on domes with a larger radius of curvature with more quadrangular cells (Kato 2014).
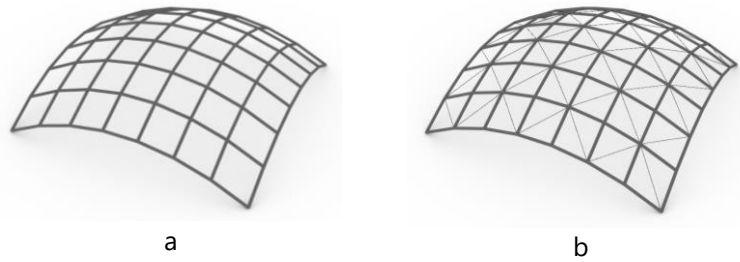
a                                              b

*Figure 4: Quadrangular grid (a) unbraced and with (b) diagonal braces.*

The triangular meshes, fundamentally, provide planar faces, and, consequently, they can have their vertices move freely for design purposes while keeping planarity. Quadrilateral meshes do not have the same freedom, as they rely on a certain set of curves to ensure planarity of faces. Triangular meshes have good structural properties, after all, the triangle is a stable shape, while quadrilaterals are not, more often than not requiring the installation of diagonal braces. Triangular panels are typically cut from rectangular sheets, which could generate more waste of glass cladding than quadrilateral mesh panels. Generating planar faces for glass cladding in complex surfaces with quadrilateral grids is more challenging, and the production of curved glass is highly expensive. A disadvantage of the triangular grids is that its nodes have high complexity. One node must provide a stable joint for six bars, while on other polyhedral grids, the nodes can be simpler, with a smaller number of bars per connection. Triangular meshes generally require more parts and are heavier than quad meshes (Pottmann et al. 2015).

Schober (2015) presents a great variety of specifications of constructed reticulated transparent shells. The recommendation for the size of glass panels is of a maximum of two to three meters. The dimensions most commonly used, though, are around one by one and a half meters. This limitation may be due to the desired curvature of the surface, to the best planarization available without making the mesh size too small, and to the warping limitation of glass.

A practical way to build quadrangular grids with planar faces is to translate a curve, the generatrix, along the length of another curve, the directrix (Figure 5a). The intersecting points of discrete translations of the generatrix provide grid points to build quadrangles with planar faces (Figure 5b) (Pottman et al. 2007).
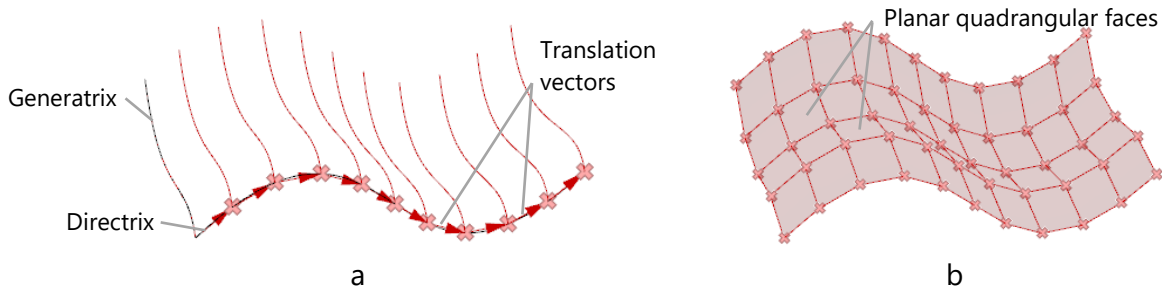
*Figure 5: Generation of a planar quad grid: (a) translation of curve; (b) mesh with planar faces.*

Dome-like gridshells can be classified due to its grid distribution. Diamond shape, Kiweet type, and ribbed type distributions are a few examples that can be observed in (Schober 2015). Figure 6 shows a variety of grid types found in constructions.
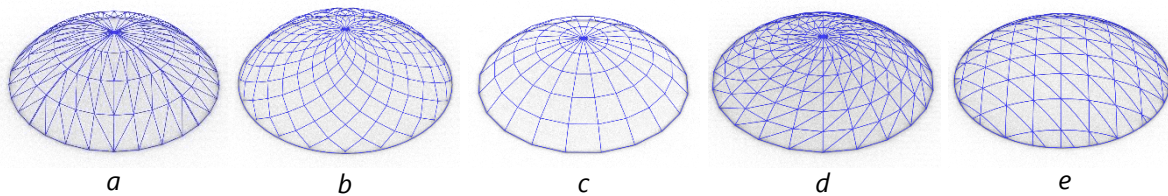


*Figure 6: Examples of grid distribution for domes: (a) Kiewitt; (b) Lamella; (c) Ribbed; (d) Ribbed with triangulation; (e) Three-way grid.*

It is good practice to avoid members that are too long since they are judged unpractical for construction (Shigeta et al. 2015).

In the present study, the triangular single- and double-layer gridshells are presented. Specifically, one double layer type of grid is studied, it is based on the vierendeel system: the lower- and upper-layer members are aligned, as showed in Figure 7. This system is aesthetically pleasing, it enables installation of equipment between the two layers and allows for larger spans than single layer structures.
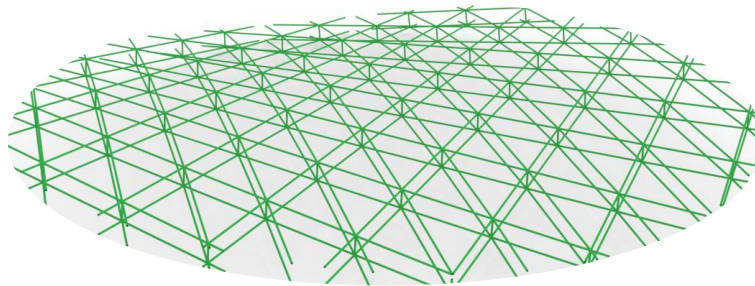


*Figure 7: Vierendeel system for gridshells*

## 3.4   Structural Analysis and Buckling Evaluation

Load cases depend on the design codes of each location, but, usually, the governing loads of reticulated structures are dead and snow loads. Wind and earthquake loads must also be considered for the project. In Brazil, without the presence of snow or earthquakes, the evaluation is focused on dead, wind and live loads.

One of the most important references for buckling evaluation of reticulated shells is the Guide to Buckling Evaluation (Kato 2014), which collects information from many studies.

Buckling is a form of a collapse of a structure, due to a critical axial loading that causes the structure to present large displacements. **Stable symmetric bifurcation** happens on straight elastic column under concentric axial compressive force. The column may, after a critical load, present displacements to one of its sides, in respect to its weak axis. If there are geometric imperfections in the column, it holds a smaller load value. This behavior is found in hyperbolic paraboloidal shells. **Unstable symmetric bifurcation** appears in rigid columns supported laterally by a spring; although the buckling path is symmetric, the load capacity decreases with displacement, instead of slightly increasing, like the stable behavior. This buckling behavior is also imperfection sensitive and can be found in thin spherical shells and circular cylindrical shells under lateral pressure or axial compression. **Asymmetric bifurcation** has a stable path and an unstable path; it is supported by a diagonal lateral spring. The unstable path is imperfection sensitive. This buckling behavior and can be found in buckling of thin cylindrical shallow panels under lateral pressure. **Limit point buckling**, or **snap-through** buckling, is found on systems similar to a shallow pin supported truss with two elements, with a vertical load on the middle point, where both elements connect. After a critical load, the structure may flip to a mirrored configuration. This behavior can be found on shallow arches, spherical caps, or extremely shallow reticulated domes subjected to large lateral pressure or concentrated loads. This buckling behavior is usually found in combination with some other pattern in reticulated shells (Kato 2014).

There are three major types of buckling in buckling load evaluation of reticulated shells: linear bucking, elastic buckling with imperfection sensitivity, and buckling strength as a global structure. The strength is defined as the resistant capacity as a global structure, including material and geometrical nonlinearities.

Buckling types in shell structures:

- **Shell-like buckling** (Figure 8b) is when the surface undulates due to buckling with displacements at nodes. It is also called global buckling. Shell-like buckling is strongly influenced by the bending rigidity at connections or nodes.
- **Member buckling**
- **Node-rotation buckling** (Figure 8a)
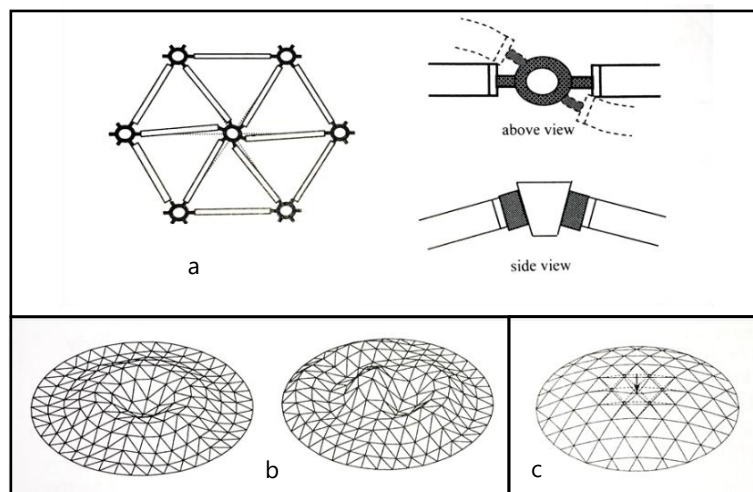- **Dimple buckling** (Figure 8c)



*Figure 8: Buckling in gridshells: local and global distributions* (Kato 2014)

Reticulated shells can present combined modes of buckling:

- Member buckling combined with shell-like buckling can appear in very slender members of single-layer reticulated shells of relatively high rise;
- Member buckling combined with node-rotation buckling can appear when connections at nodes have relatively low bending stiffness (Kato 2014).

While shell-like buckling is the main factor influencing design in single layer grid shells, the member buckling appears as critical buckling in double layer grid shells, prior to shell-like buckling. However, in cases where depth between upper and lower layers is very small, shell-like buckling likely appears. It is common to model pin-connections in double layer grid shells, but a detailed analysis of the connection's rigidity may provide good information for modeling semi-rigid connections, with some bending capacity. This increases slightly the buckling load of the structure.

Design of elements in reticulated shells can be related to the design of a column subjected to buckling, through the choice of a **representative member** of the structure, with proper choices and adaptations of buckling forces. For instance, the axial elastic buckling force should be adopted considering the effect of design imperfection.

Several design factors influence the buckling resistance of gridshells. Reticulated shells resist external loads through membrane action with low bending moments, reducing chances of shell-like buckling, which is strongly dependent on the geometry. **Boundary conditions** also influence buckling strength: pin supports provide higher buckling resistance than simple supports, which in turn provide higher resistance than free edges. **Members**, **nodes**, and **connections** are additional three factors for evaluating buckling in a gridshell. The member's slenderness ratio, subtended half angle, and its arrangements provide details on the type of buckling that may appear; as well as rigid or semi-rigid connections applied to the model.

**Geometric imperfection** can appear as nodal deviations, affecting global buckling strength; and as member crookedness, affecting local buckling strength. Other types of geometric imperfection can be initial looseness of connections, eccentricity at connections, and discontinuity of gravity centerlines. The last two types may be modeled as induced bending moments at nodes. The global geometric imperfection is usually the most influential factor to the buckling strength. **Load distribution** is another factor that affects buckling loads. Lastly, **initial tensions** can stabilize or increase the strength of the structures; such as initially pre-stressed braces, which provides in-plane shear rigidity. (Kato 2014)

Structural analysis of reticulated shells can include, at first, linear models, for both geometry and material. For more detailed analyses the consideration of either geometric nonlinearity or material nonlinearity, and later, both, may provide better knowledge of the structural behavior.

The guide to buckling evaluation (Kato 2014) presents detailed information for reticulated shells with more conventional forms, such as spherical caps and cylinders, however, for free form reticulated shells, the information is still limited for the buckling evaluation. The guide presents a general procedure with different types of analysis. A flowchart is presented, and it is organized in eleven steps. The steps are separated in checkpoints for compliance, and in routes defined by these checks.

Structural analysis of the connections of the reticulated structure should also be conducted thoroughly, with different load combinations for a deep understanding of its behavior. The study by Ma et al. (2017) shows analyses of pure bending, normal tensile and compressive axial load both with and without eccentricity, and a combination of bending and axial loads. The study is parametric and provides detailed information for the application of the developed joint system.

Buckling loads in reticulated shells can be studied through an optimization perspective, where higher loads are desired with less use of material. The optimization problems can be solved with a variety of methods; here, the genetic algorithms are studied.

## 3.5    Structural Optimization

Structural optimization, in short, consists of rearranging design variables to find an outcome, with the required objective functions, that meets the applied constraints. Commonly, in gridshells, it consists of the rearrangement of structural members in space to find a stiffer and lighter structure that meets safety criteria. There are many methods to optimize a structure, and the following concepts described are common to most optimization processes and can help on the choice of a method.

- *Design variables*: what can we change to find the optimal solution?
- *Objective functions*: what goal do we want to achieve?
- *Constraints*: what are the conditions that limit our search space to find feasible solutions?

The optimization methods vary from mathematically defined functions, where maximums and minimums can be evaluated; to calculus-based techniques, where stochastic methods are used. The latter is used for highly nonlinear processes, thus, it is suitable for gridshell optimization problems (Dimčić 2011).

There are two broad groups in the optimization of structures: one is single objective optimization, the other has more than one objective than one (multi-objective optimization). They are both described in Sections 3.5.1 and 3.5.2.

Another important concept in the optimization of structure involves the main goal and restrictions of the project. A project may require an area that needs covering, without specified surface form. In this case, an optimization study of surfaces, like in Figure 9, can be conducted. The study includes different support conditions in this example. The project may, however, come with a predefined surface to which the structural system needs optimization (Adriaenssens, Block, et al. 2014). The problem is depicted in Figure 10. Both optimization processes are important. The one regarding shape optimization was presented in Section 3.1, the grid distribution in a predefined surface is now explored.
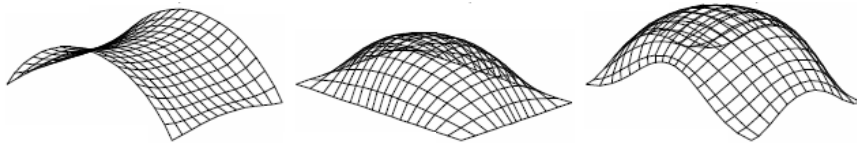


*Figure 9: This illustrates optimization that allows for support condition variation and for surfaces to change the geometry* (Shigeta et al. 2015).

In Figure 10 the angles between rods, the refinement, and orientation of the global configuration of the mesh are in question.
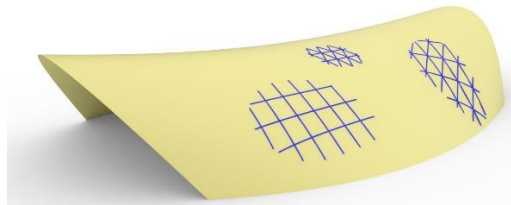


*Figure 10: Mapping and optimization of the grid on a given surface*

### 3.5.1 Single objective optimization

There is one main objective to achieve in this type of optimization, where the design variables are changed until one predefined goal is met. In this case, there is usually a single best option that has better properties than any other tested option. An example of a single objective optimization is to minimize the weight of the structure while keeping safety criteria as a restraint. The optimization algorithm, then, changes the cross-section of the element and performs structural analysis. Then, it calculates the weight of the structure and the maximum displacement or tension allowed. The algorithm iterates with different characteristics

depending on the optimization method, but the outcome is one structure that performs better than any other tested. It is often the case when other objectives, such as maximizing the stiffness in combination with maximizing the buckling load, are interesting to achieve; leading to multi-objective optimization.

### 3.5.2 Multi-objective optimization

There are usually two or more conflicting objectives in multi-objective optimization. An example (Deb 2001) presents a cantilever beam with a concentrated load applied at the end of the beam (Figure 11). The design variables are the length of the beam and cross-section diameter. The objectives are to minimize beam weight and end deflection. The constraints limit maximum stress and deflection.
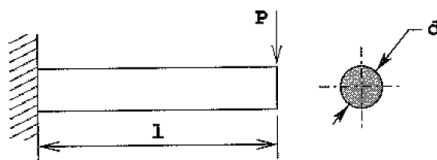


*Figure 11: A schematic of a cantilever beam and its cross section* (Deb 2001).

It is intuitive to say that the smaller the cross-section diameter is, the smaller the weight of the beam, however, the end deflection increases. On the other hand, the bigger the diameter of the cross-section, it has less deflection, but it is heavier. One solution is not better or worse than the other regarding both objectives, this is a *non-dominated* solution. If these solutions are plotted in a graphic, it would form a curve known as the Pareto-optimal front, seen in Figure 12. The longer the length of the beam, the higher the deflection and weight. These set of solutions are, as a matter of fact, worse than the ones on the Pareto front for the given problem.
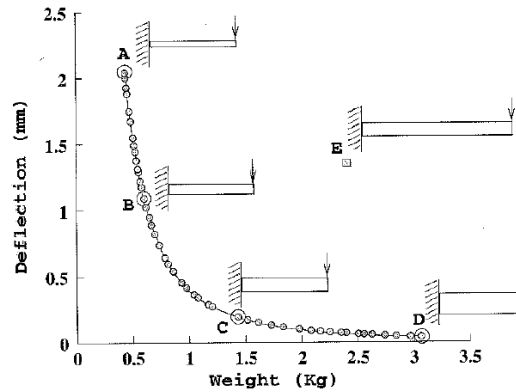
*Figure 12: Four Pareto-optimal front solutions and one non-optimal solution* (Deb 2001).

The solutions on the Pareto-optimal front are also known as tradeoff solutions. The solutions in this set are better than all other solutions with respect to at least one of the multiple performance objectives (Winslow 2014).

There are many other cases where the problem is higher in complexity and are not as intuitive as this example. The parametric tools can be very helpful in finding possible outcomes, so the designer can, then, choose what they are looking for. One example of high complexity multi optimization study is (Yang, et al. 2015), where daylight, energy and structural performances are studied together to help decision making in early phase design.

Another example is a study by Shigeta et al. (2015), it shows that a lot of the studies in lightweight spatial structures consider optimization of strain energy, stresses and buckling loads either through cross-sectional optimization or shape optimization, but not both. It is proposed that both member stiffness distribution and shape optimization be used to find a spatial structure with higher buckling strength than if it was only created with shape optimization. Four different procedures are applied. To build the different procedures, the order of each of the three types of optimization are varied. The optimizations are shape, stiffness distribution, and simultaneous shape with stiffness. These are conducted through variation of initial shapes, degrees of freedom of the surface's control points, boundary conditions, and loading conditions. A single layer rectangular reticulated shell generated through a Bezier surface (Pottman et al. 2007) is used for the numerical example. The grid division of the surface is also variable to allow for members of similar length even with higher curvature.

In cases where the surface is given, applying form-finding methods mentioned in Section 3.1 is not an option. Rearranging element distribution on the surface may be the best way of improving structural efficiency. For such optimization, the mapping of the grid (Winslow 2014) must be generated with relevant parameters that allow for different orientations of the mesh, refinement, and spacing. The values for the constraints might include a certain angle between bars, or equal length bars, and so on. The evaluation of the generated pattern might need to consider the constructability of the structure, besides its buckling resistance and any other criteria.

Structural optimization has been characterized through mesh refinement, the pattern of the mesh, sizing of elements, the variation on the distribution of the grid, placement of supports and the form of the discretized surface itself. One other way of optimizing the gridshell is testing different topologies, taking elements away in some places, and checking for the objective parameters, such as the total weight of the structure. This is called discrete topology optimization, an example of it applied with the use of genetic algorithms (Section 3.5.3) can be found in  (Richardson et al. 2013), and a major issue pointed out is the need to verify mesh connectivity and structural stability.

The genetic algorithms (GAs) are instrumental in problems where there is a wide range of options. Slight changes to the found form can be applied to explore differences in member orientation and their relation the form. GAs components are also a part of  the parametric programming software. They are further explained in Section 3.5.3, but they rely basically on well-defined objective functions and variables. Objectives may vary from a maximum allowed deflection to the relation of light to shaded area desired in respect to element orientation. Variables can be determined as the vertical component of the surface's control points, variation in the spacing between elements, or a different number for mesh refinement. Constraints of the defined problem restrict the search space of the algorithm; they can vary from types and predefined locations of support conditions to the size of paneling elements.

### 3.5.3  The Genetic Algorithms

"In the 1950s and the 1960s several computer scientists independently studied evolutionary systems with the idea that evolution could be used as an optimization tool for engineering problems. [...] Genetic algorithms (GAs)

were invented by John Holland in the 1960s and were developed by Holland and his students and colleagues at the University of Michigan in the 1960s and the 1970s. In contrast with evolution strategies and evolutionary programming, Holland's original goal was not to design algorithms to solve specific problems, but rather to formally study the phenomenon of adaptation as it occurs in nature and to develop ways in which the mechanisms of natural adaptation might be imported into computer systems." (Mitchell 1998).

GAs can solve a great variety of problems that need not be defined in detail. Although it has slow convergence rate, it is readily available on the computational environment chosen, it is widely used in the research community, and proves itself reliable, given the right precautions to avoid local optimum is taken.

Some of the most common definitions in GAs are:

- Chromosomes: strings of zeros and ones, or "bits", composed of genes (the bits), and each gene is an instance of a particular allele (zero or one).

- Population: a collection of chromosomes. The population is updated after one round of the iteration process.

- Natural selection: involves a selection operator that defines the chance of a chromosome to reproduce. The fitness score of the chromosome defines if it has more chances of reproducing than other: the fitter it is, the more offspring it is likely to have.

- Crossover: certain subparts of two chromosomes are exchanged, creating offspring that will be part of the next population.

- Mutation: random changes to allele values of random locations of the chromosome, usually with a very low probability of occurrence.

- Fitness function: a function that assigns a score to each chromosome in the population, the fittest tend to have higher chances to reproduce. "The fitness of a chromosome depends on how well that chromosome solves the problem at hand." (Mitchell 1998)

In a discrete system composed of $k$ number of bars and $m$ number of nodes, the nodes could be defined by three cartesian coordinates ($x$, $y$, $z$), as an example. In this case, a gene could be one number that is set as the $z$ coordinate of each node, forming a collection of $m$ number of genes in total. The collection of $m$ genes composes a chromosome, and the collection of different chromosomes composes a population. One run of a GA can include a population of

50 chromosomes, for example, and usually there are numerous runs until the algorithm converges to a set of results.

In gridshell studies, the GAs can be used to rearrange the grid pattern and spacing in a certain way that stresses on each bar and node are smaller. Furthermore, the angle in which the bars enter the nodes needs adjustment, they should be as similar as possible to avoid node rotation.

An example of steps of a flow chart for a problem about the direction of the grid geometry (Winslow 2014) solved using a GA is:

- Convert NURBS to triangulated surface mesh
- Input parameters (rod spacing, member sizes, load cases, objectives)
- Randomly generate 100 sets of rod directions (gen = 1)
- ♦ Generate 100 different grid geometries
- Build Finite Element models
- Evaluate two objective values for each grid geometry (buckling and deflection)
- Is generation (gen) >100?
- If yes, end. If no, follow to next step
- Selection → crossover → mutation → (gen = gen + 1) → return to ♦

It is clear in the steps of the flow chart by Winslow (2014) that the algorithm is iterative, and that the population of individuals and the number of generations cannot be too small in order to avoid producing a nonrealistic local minimum instead of global (100 generations of 100 individuals). The variable crossover probability in the cited work was 75%, and the variable mutation probability was 5%.

Some algorithms (Sinha et al. 2014; Danhaive and Mueller 2015) may allow for a limited number of designer choices for certain desirable structures at a designated point in the flow chart.

## 3.6   Connections

An investigation of a variety of existing structural systems for gridshells is presented. The Geometrica and Triodetic systems are the focus of the present section and can be found in the

subsection below. This study includes different manufacturing techniques, from bolted and welded metallic connections to 3D printed[4] ones.

There is an enormous variety of connection types for gridshells; some can be observed in Figure 14. For each one there are strengths and weaknesses, usually being: the more rigid and versatile the connection is, the more expensive it gets to manufacture it; or, the cheaper it is, the more unreliable or limited it gets. Being versatile or limited is mentioned in respect to different angles between bars and possible surface curvature that the system can prove solutions to.
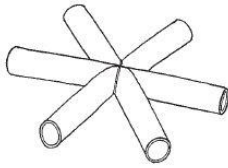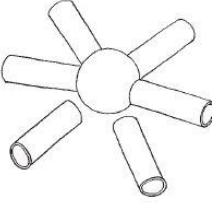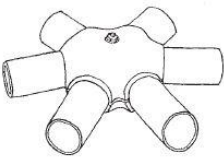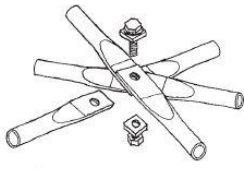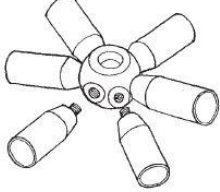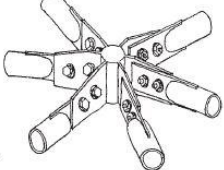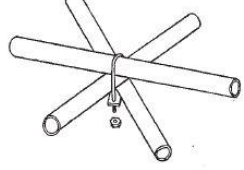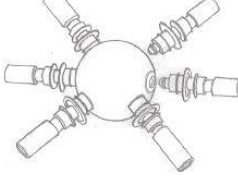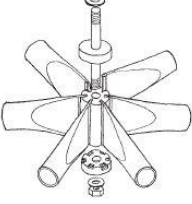
| | direct connection | node for connection | |
| --- | --- | --- | --- |
| | | spherical node | special type |
| welding connection | (a) tubular joint | (b) welded ball joint | (c)    SDC system |
| bolt connection | (d) bolt connection for flattened node | (e) screw ball joint | (f) gusset plate and bolt |
| U bolt, fit jointwedge | (g) U-bolt  (Lederer dome) | (h) spherical fit joint | (i)    triodetic system |

*Figure 13: Connections for reticulated structures. Drawing in* (Kato 2014, p.26)

---

[4] 3D printing, also known as additive manufacturing, became widely available around 2011 through a desktop machine that prints a continuous filament of a thermoplastic material. The most popularized process is called fused filament fabrication (FFF). The machine extrudes filament from a heated head that moves through a table (bed) depositing material in predetermined planar coordinates, and once a layer is complete, the heated head is moved upwards and starts depositing the next layer (3DHUBS 2019).

The screw ball joint, shown in Figure 14, is a great example of a highly versatile, and structurally sound node that can be applied to many different types of structures. It is, however, known to be quite expensive, especially in Brazil, turning some constructions unfeasible.
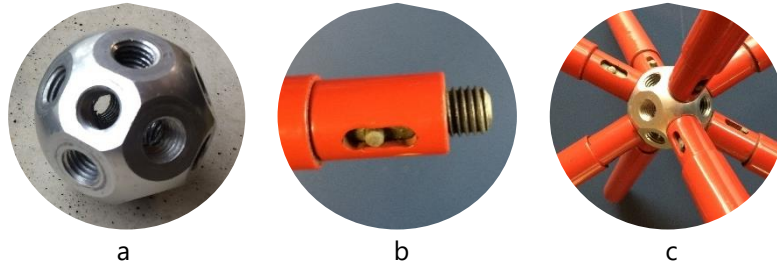


a                              b                              c

*Figure 14: Screw ball joint: (a) node; (b) detail of the bar end; (c) bars connected to node.*

The flat-end bars, shown in Figure 15a, that are joined with a bolt is inexpensive, however, structural safety uncertainties surround this type of system (Maiola 1999).
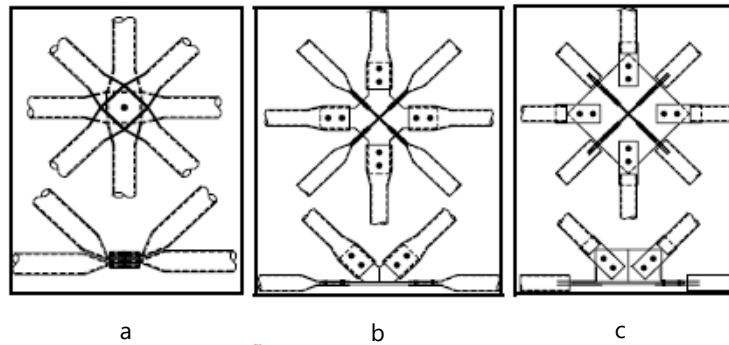


a                              b                              c

*Figure 15: Connections with flattened end bars: (a) typical flat ends; (b) flat ends with gusset plate; (c) ends with stiffeners and gusset plates*

Oya et al. (2016) show buckling behavior on members connected with gusset plates (Figure 15b, c), also a common connection with the use of flat-end bars. The paper indicates a large variety on the tests, indicating the buckling length in such cases should be larger. High safety factors are needed for these connection systems.

When searching for patents, it becomes clear that the gridshell structural systems have not only been around for a long time, but they are constantly developed over the years. There are options ranging from robust, intricate, structural systems for space frames (screw ball joints), to ideas that are possible to be made by anyone with a simple set of tools, and explained in do-it-yourself tutorials on video-sharing websites (Zip Tie Domes 2017; Build With Hubs 2017). It is only natural that, with the ever more available manufacturing techniques, new types of systems will be developed. For now, there are metal printed joint systems, they use topology optimization, which allows the use of less material (Kassabian, Cranston, and Lee 2017).

The SmartNode (N. Williams et al. 2015) project also uses 3D printing with nodes generated using topology optimization. This type of optimization involves withdrawing material from the least solicited parts of the domain. Topology optimization has been largely used by automotive and aerospace industries for manufacturing lighter and stiffer structures. In recent years the manufacturing techniques used for these industries have been further explored by the civil engineering industry, especially with the broader availability of additive manufacturing techniques for printing concrete, and metallic materials. New nodes for lighter structures have been developed with such available algorithms and construction techniques.

Connections can also be fabricated with formwork produced by laser cutting machines and later filled with resin or any other appropriate material ("Architecture+Fabrication: MakeTANK" 2018). A negative side to this may be that a lot of different nodes are needed for a complex surface, and a large number of different formworks would be required. However, it may be the case where a certain formwork can only be used for a limited number of times, so if there is a small repetition on the nodal geometry then this procedure might be just right for the structure.

Entirely printed nodes are aesthetically pleasing, and they provide solutions for structural problems that fall out of what is commonly seen in projects. An example of this is the stadium façade that has numerous unique panels that need to be attached in a singular way to the support structure (Warton, May, and Kovacevic 2017). The solution presented a printed node with a central hub that had notches for the interconnecting "arms" (the arms are printed parts between metal façade plates and the hub). These notches were produced with a unique interlocking mechanism between notch and arm such that if a wrong connection were to be attempted, the arm would not fit. This is a sophisticated solution for a large and challenging project. Printing all the nodes has its downsides, nonetheless: it is still very time consuming, and some software incompatibility adds still more time for the whole process. Printing speed is limited by material properties. Regulation and quality control of these printed materials are also important. Fast, high precision, with engineering materials machines are still expensive and cost prohibitive for many applications.

There are many other types of nodes, but one that stands out is the one developed by Triodetic and Geometrica companies because its cost tends to be lower when compared to MERO

system (a patented screw ball joint), and they developed a way to cover a great variety of surfaces.

### 3.6.1 Geometrica and Triodetic systems

Both Geometrica and Triodetic systems are very similar, they consist of triangular meshes with circular hollow bars with flat ends that are fixed on a cylindrical hub, as shown in Figure 16. The details on the connection parts have differences, but the main concept is the same: be able to provide a structural system solution with one standardized hub and varying bars lengths and flattened ends parameters. There are three types of parameters on each bar described in the following sections: length of the bar, coin angle, and twist angle.
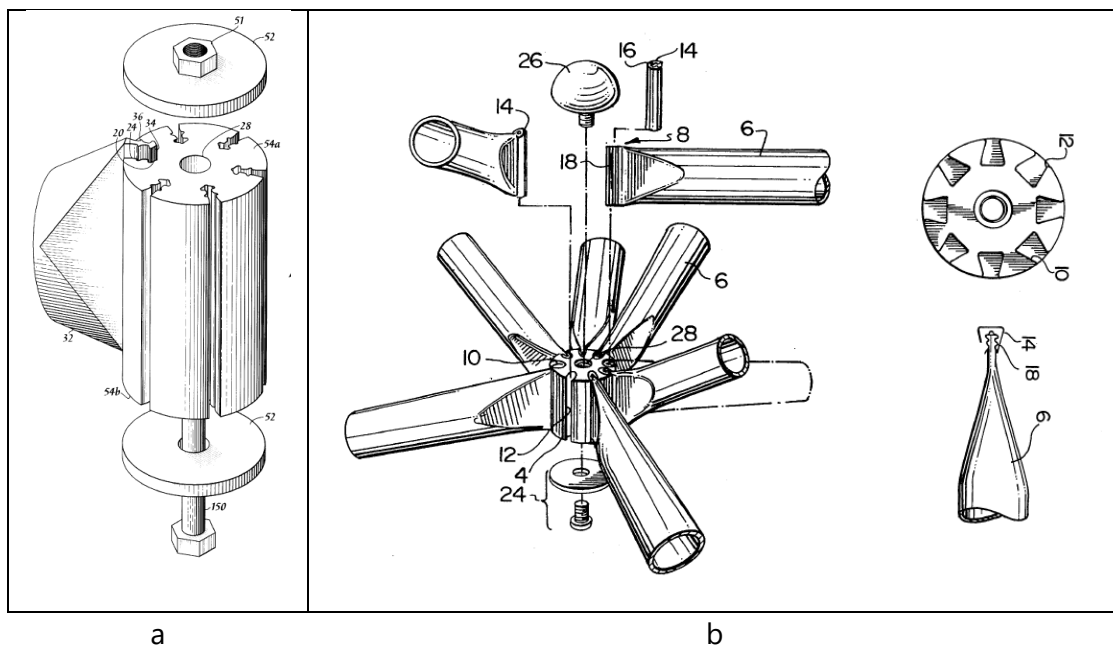


a                                                                      b

*Figure 16: (a) Geometrica and (b) Triodetic systems*

### 3.6.2 Bar length

In double layer domes, the difference between the lengths of bars in different layers can create a curvature. For example, if the bars on the lower layer are all smaller than the ones on the upper layer, then the surface would be dome-like. If the lengths of the bars are varied in different ways along the surface, the structure can have different curvatures. Although lengths can be different, it is recommended that the size of the bars are not extremely different from its adjacent ones to avoid buckling of longer members.

### 3.6.3 Coin angle

The coin angle (Figure 17) is how its flattened edges are "sliced" – vertically at both ends, or at a certain angle. With this property, it is simple to insert a diagonal bar that goes from one layer to another without having to change the node.
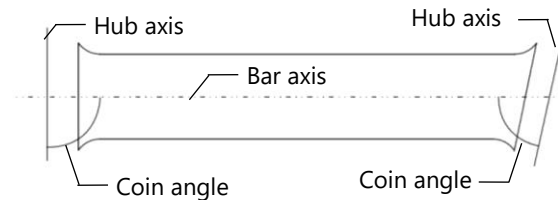


*Figure 17: Coin angle* (Kato 2014)

### 3.6.4 Angle of twist

The flattened ends of the bars can be made with the vertical lines aligned, or with a certain difference between them, considering the longitudinal axis of the bar as a reference. This means a bar could be inserted in a vertical node on one side and on a rotated node in relation to the bar axis on the other without having to change the geometry of the node. This is the twist angle: the difference of angular alignment between flattened ends of the same bar (Figure 18).
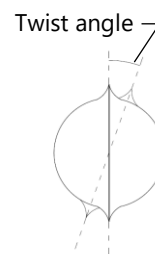


*Figure 18: Angle of twist*

### 3.6.5 Nodes

The nodes, or hubs (Figure 19), are standardized, they are cylindrical, with a central hole and vertical notches towards the outer surface of the cylinder for the bars to enter. The central hole allows for a vertical pin to enter and a vertical bar to be attached, joining lower upper layers. The number of notches in each hub varies from the Geometrica system to the Triodetic one, and other attachment details as well, however, the main description of the structural system is the same.
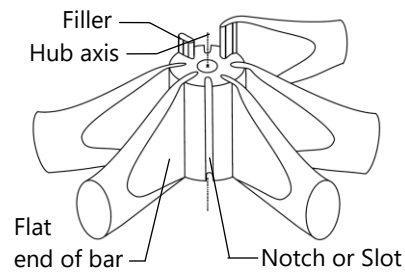
*Figure 19: Hub* (Kato 2014)

This system can solve a variety of surface shapes, the company's website (Geometrica n.d.) shows how flexible the system can be.

# 4 Proposed gridshell system

The previous sections presented a variety of specifications that are extremely relevant for gridshell design and construction. They are not all used in the process of creating and evaluating this system, they are, nevertheless, what allows the comprehensive creation of this system and the knowledge to proceed into future steps. Without the previous study, this would not have been developed the way it was. Understanding that the choice of cladding interferes with the maximum size of members (glass usually is no longer/wider than 2 meters) is key to developing a system for such cladding. Just as understanding the variability of mesh properties and how they are generated is key to using its extrusion properties, to dealing with torsion in members, and other parameters. Implementations of optimization algorithms, structural analysis evaluation of parameters and proper evaluation of the system's design are all known to be necessary, however, not in the scope of the present study.

While the inspiration comes from the Geometrica system to build a prototype, the actual proposed system has some differences. The first issue with the existing system is that it uses flat end bars: that process reduces section properties and makes it prone to micro fissures along the edges of the flattened ends. Those fissures could compromise the material for corrosion if other measures are not taken. Flat end bars can make the system easier to produce and to build, but a proposition of a system without that characteristic would be ideal. Figure 20 depicts the problem of connecting a standardized hub to a tubular bar with varying surface parameters.
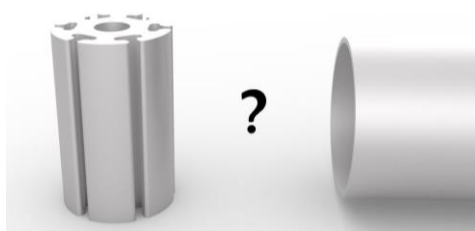


*Figure 20: Connection problem definition*

Apart from the initial creative process and programming the geometries there are two major design phases in the development of this structural system. First, is proving the concept created in the computational environment on a small scale, and second, is developing a prototype with final materials and geometries to build a one to one scale pavilion. This dissertation focuses on the first phase: the proof of concept (Bisplinghoff 1969). Although the

solutions provided for the system are applied to a small-scale physical model, the experience is expected to provide a greater understanding of issues and processes that structures like gridshells present. Scalability of the model and possible solutions are discussed in Section 6.

Concern for future development of the connection system is present, and variable parameters are implemented in the parametric definition for wide applicability. Following, steps for creation and programming of the connection system are detailed in subdivided sections.

## 4.1  Concept for the structural system

The gridshell node comprises of hubs and interconnecting parts; the latter connect the hubs to the bars. The interconnecting parts absorb most of the different parameters of the structure. Interconnecting parts may be all unique in a structure. Alternatively, the structure may be optimized to have a limited amount of different interconnecting parts. The hubs are the standardized elements of the structure, with notches distributed around its edges. One structure may have more than one type of hub. Figure 21 exemplifies a six-notch hub.
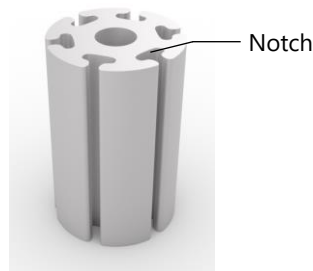


*Figure 21: Conceptual configuration of a six-notch hub*

The hubs are the cores of each node. As a node increases in size, the hubs may have larger diameters and heights. The interconnecting parts, however, should be just the required size such that it absorbs the different parameters of the connection. These parts should not increase considerably for larger connections, as the hubs might need to increase. There are a few reasons that the hub and interconnecting pieces are different elements, and not modeled as one entire node. The reasons are related to the choice of using 3D printing machines to produce the proof of concept model; after all, it is, currently, the most efficient way to produce many pieces, each with different geometries, for small scale production. The first reason for separating the node into two types of elements is that 3D printing is time-consuming; consequently, it is advantageous to print the least possible material. The second reason assumes larger scale models will also use 3D printing machines; as the printed piece is limited

to the bed size of accessible machines, it is advantageous to have smaller interconnecting parts, rather than 3D printing the entire node. A third reason is that, if there are spare or recycled parts from other structures which could be used as hubs for a new project, then it would be possible to create a different structure only by adding the interconnecting parts to the project.

Although the proof of concept uses 3D printing for the interconnecting parts, these parts may be produced through milling, casting, or other available processes.

The connection system is intended to be easily assembled, disassembled, and reused. The parametric definition will include different bar cross-sections for the grid members in future works (Section 7.1).

## 4.2    Hub choice for the current development of the system

The profile for the hub can be extruded with any given parameter for fabrication. The one used for the proof of concept (Figure 22) is found in the market for sale; it is primarily used for fairs (career fairs, science fairs, etc.). For the first phase of the design process, the hub geometry found is used for the programming steps as well.
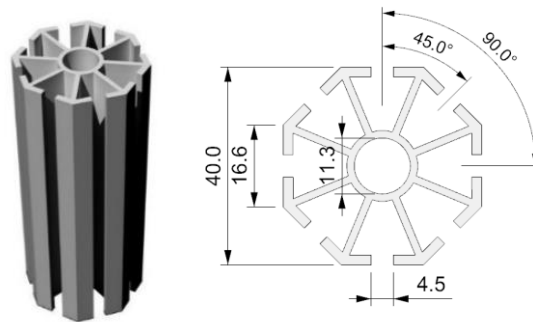


*Figure 22: Extruded aluminum profile used for the hub. (length units in mm)*

## 4.3    Global and local definitions

The grasshopper definition of the geometries has two parts. The first is a global definition of the mesh, support locations, and angles between bars. The second part is a local definition of the connection geometry, which takes the global mesh as input. The local and global parts of the model are closely related. For instance, if the hub accepts up to four bars, the user should generate a quadrangular mesh, and not a triangular one, which usually requires six bars per

hub; and if the scale of the mesh is larger, then the hubs and pieces must be adjusted accordingly.

The global gridshell model must be structurally stable, and, for this part, the designer might benefit from form-finding techniques, such as dynamic relaxation, or force density method, in such a way that the bars and nodes might require lower structural capacity for a given load. Additionally, discrete topology optimization methods for the positioning of the bars can reduce material usage (Richardson et al. 2014). Figure 23a shows a cylindrical surface discretized into quadrangles, where angles between mesh edges are measured on the screen allowing for immediate adjustments by the designer. An offset was applied to the mesh to generate the second layer. Figure 23b shows the mesh was used to generate the local geometry of the interconnecting parts. The generation is automatic, and given parameters are adjusted for the scale of the model and quantity of notches allowed in a hub.



*a*  *b*
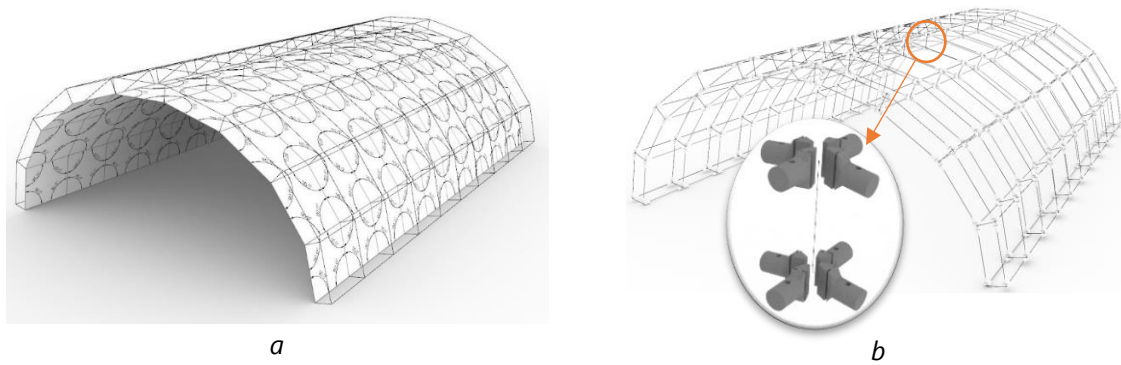
*Figure 23: Quad mesh on a cylindrical surface: (a) global discretization of surface considering angles between edges; and (b) geometry of interconnecting parts generated on corresponding connection locations.*

## 4.4   Connection system

A preview of what the connection system looks like for a single and a double layer gridshell is in Figure 24. A single layer connection system is in Figure 24a; a double layer type of connection with short distance between layers is in Figure 24b; a double layer connection system with  longer distance between layers and with a diagonal member is in Figure 24c; and the double layer connection is shown in a side view in Figure 24d to demonstrate the twist angle between nodes.
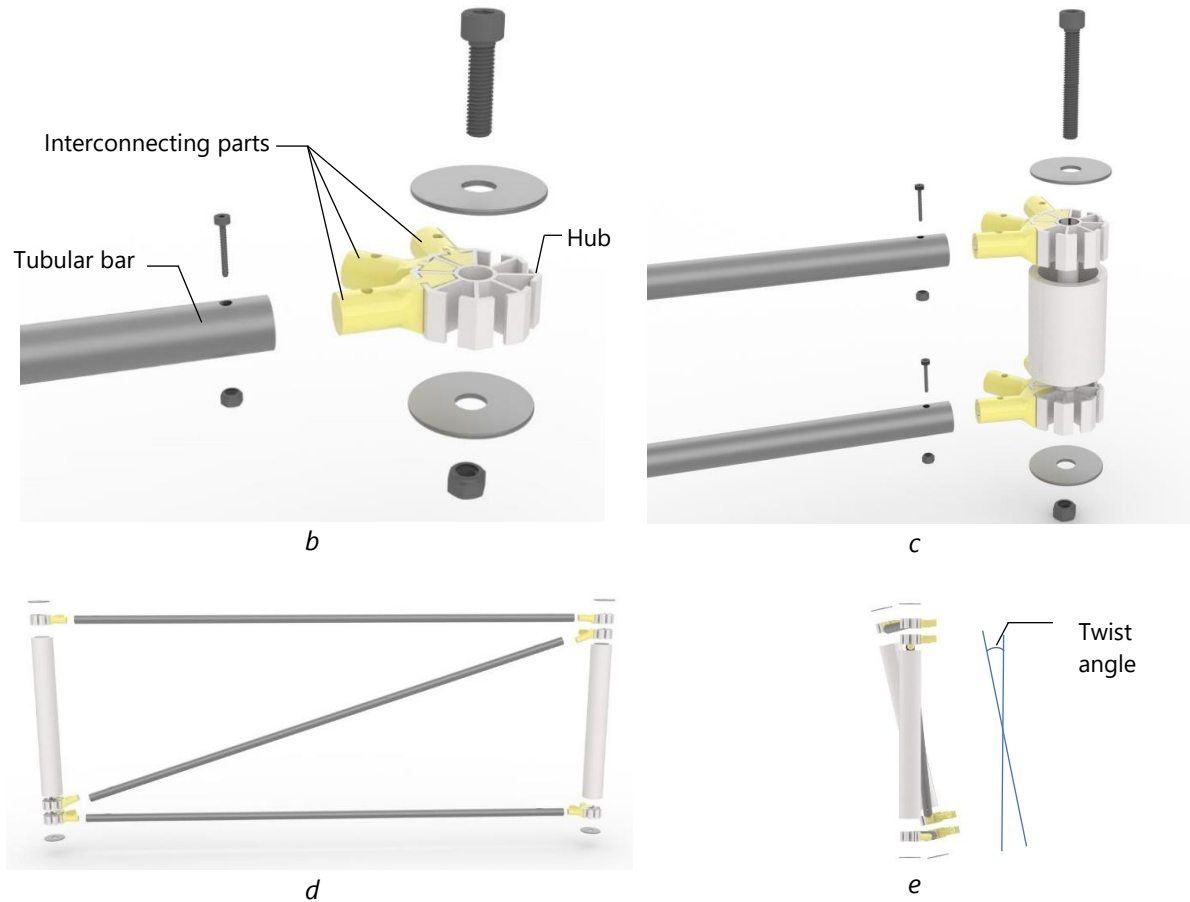
Figure 24: Connection details and variations: (a) single layer; (b) double layer - shallow; (c) double layer - deep; (d) double layer with torsion.

The programmed local geometry cluster can be set to produce geometries for hubs with a different number of notches, or for one only, as needed. The choice of the hub when more than one type of hub is allowed is given by the smallest distortions of pieces possible. This is further detailed in Section 4.11. Figure 25 exemplifies the interconnecting parts distributed in space for hubs with different numbers of notches: four (Figure 25a); five (Figure 25b); six (Figure 25c); and eight (Figure 25d).

|  c  |  d  |
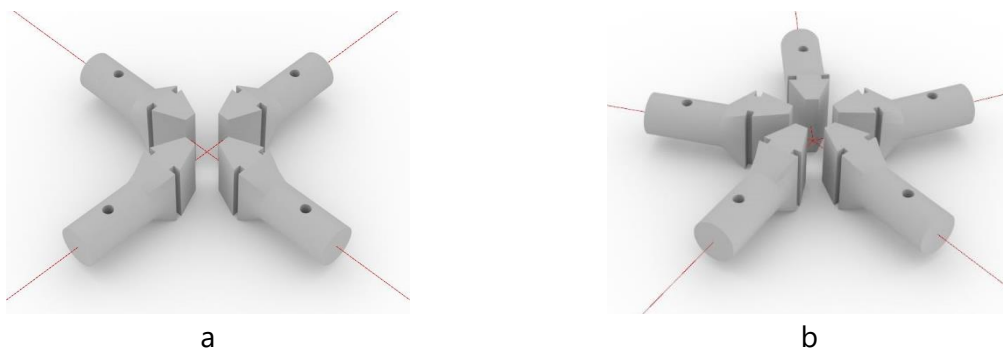
*Figure 25: Interconnecting parts distribution according to node: (a) four notches; (b) five notches; (c) six notches; (d) eight notches.*
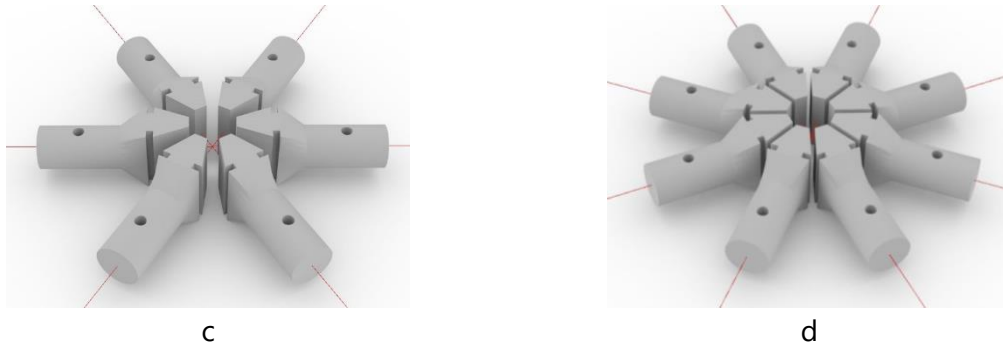
## 4.5    Mesh generation

After choosing the type of the hub, the mesh is generated on the chosen NURBS surface. The generation of the mesh can be made through components and add-ons within the parametric software. The method to generate the mesh may alter the way it can be modified in optimization algorithms in later studies.

A quad mesh can be created with a component subdividing the surface in directions $u$ and $v$ of a NURBS surface. $U$ and $v$ parameters and the control points can be observed in Figure 26. A component from Mesh+ (NeoArchaic 2018), for instance, allows for triangulation of quadrangular meshes. This triangulation component takes integer inputs to define if the triangulation is made with all diagonals on the same direction, with quad elements divided on the shorter/longer distance, or with quad elements divided for the smallest/greatest area. This provides already a versatile way of varying the mesh configuration using number sliders. This number slider, in the future, could be used as a variable for an application of GAs.
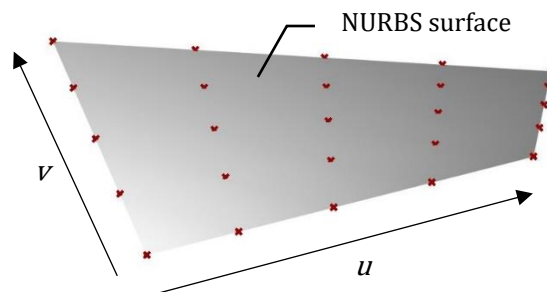


*Figure 26: u and v parameters of a NURBS surface and the control points*

Another way of generating the mesh is to build two curves, the first curve can be divided in any desired number of segments, the second curve can be copied to the division points on the first curve. This is used to build developable surfaces, as shown in Figure 5. Each curve is divided into a defined number of parts, not necessarily the same number. If there is a need to later triangulate the mesh, these segments of line may be converted into a mesh, and the same component of triangulation from Mesh+ may be used. This extra step in building the mesh may produce an opportunity to create another number slider for the variation on the distance between elements, and be used for genetic algorithms as well as described next, and represented in Figure 27.

First, a curve can be created in the direction of the elevation of the mesh, with any number of desired control points. This curve can be divided into equal lengths, and each node created can be projected onto the original structure's generating curve. Each projected node is the new mesh *u* or *v* direction divisor. This way, we can vary the elevation of only a certain number of control points, and all of the spacing of the mesh is altered.



<div align="center">a       b</div>
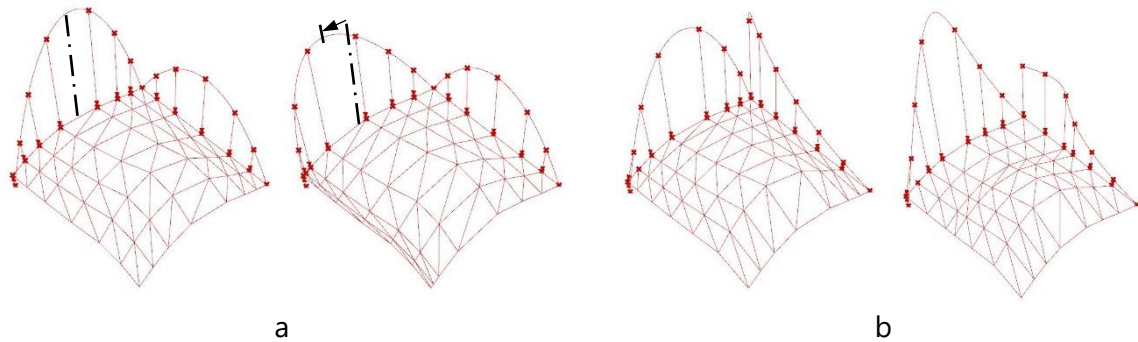
*Figure 27: Varying grid element sizes through variation of control points of curves: (a) parabola; or (b) NURBS.*

It can be, first, introduced as a parabola, with one control point. Soon we see that the grid gets spaced out in the middle and elements get clustered over the edges. The elements never get clustered in the middle. This leads to the exploration of a new curve that may allow for that, but without increasing the number of control points by a lot. The more variables a GA has, the longer it takes to converge.

A method to generate planar quad meshes is presented in (Mesnil, Douthe, Richter, et al. 2018), the method is called Marionette Meshes.

Another way to generate a mesh is to project a planar grid onto the intended surface. The intersecting points of the curved segments can be used to connect the respective lines.

No matter the way the lines of the mesh are generated, they must, in the end, be converted to a mesh to apply the offset. The mesh is the input the programmed component expects to receive.

## 4.6    Stability Analysis

This is where the stability of the structure is calculated in the Grasshopper add-on Karamba (Preisinger 2013). The mesh is decomposed in lines and nodes to be converted into truss elements and support locations. Given the geometry of the node, the connection has a fragile section near the hub notch. A semi-rigid model is created, where the rotation stiffness applied to it are very low, in favor of safety.  A default material of aluminum is chosen in the program. A non-linear analysis is available for large deformation of structures and global buckling evaluation is also available. Figure 28 shows the Karamba visualization, this structure, specifically, is used for the physical model shown in Section 5.1.

The rotation stiffness of the connections is unknown in the present study, so a very small valued is applied to simulate the semi-rigid model. Figure 28 shows the location of the supports with the arrows at the four corners of the structure, the vertical load of 1 kN added to gravity, and the defined rotation stiffness applications.
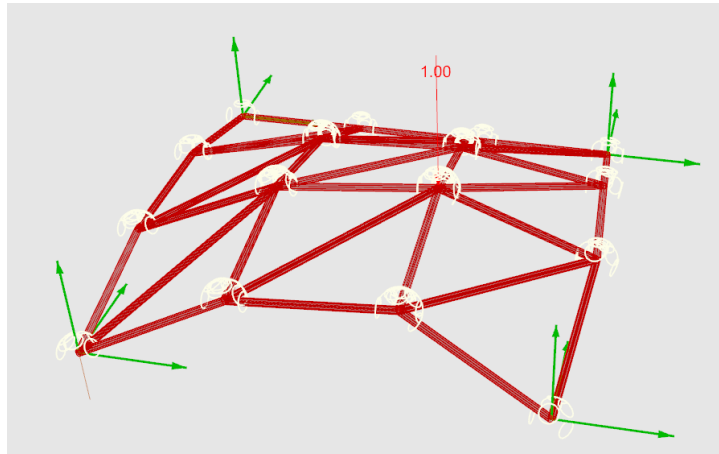


*Figure 28: Semi-rigid model boundary conditions.*

Figure 29a shows the results for axial force, with a maximum of 0.69 kN in compression, and a maximum of 0.94 kN in tension. The two compression values are circled since those are the members the local buckling evaluation should be checked. The member with the highest compression should be checked, as well as the longest element in compression, which is the bar with 0.65 kN in compression. Figure 29b shows the total displacements of the nodes. The

highest displacement is circled, it is 0.34 cm. The total displacement result is satisfactory since it is below span/250. The global buckling evaluation provided a factor of 8 to the first buckling mode.



Figure 29: Results and boundary conditions for semi-rigid connections: (a) axial force (kN); and (b) nodal displacements (cm).

A brief structural analysis of the global system was shown in this section. This allowed quick dimensioning of the physical model and its successful production.
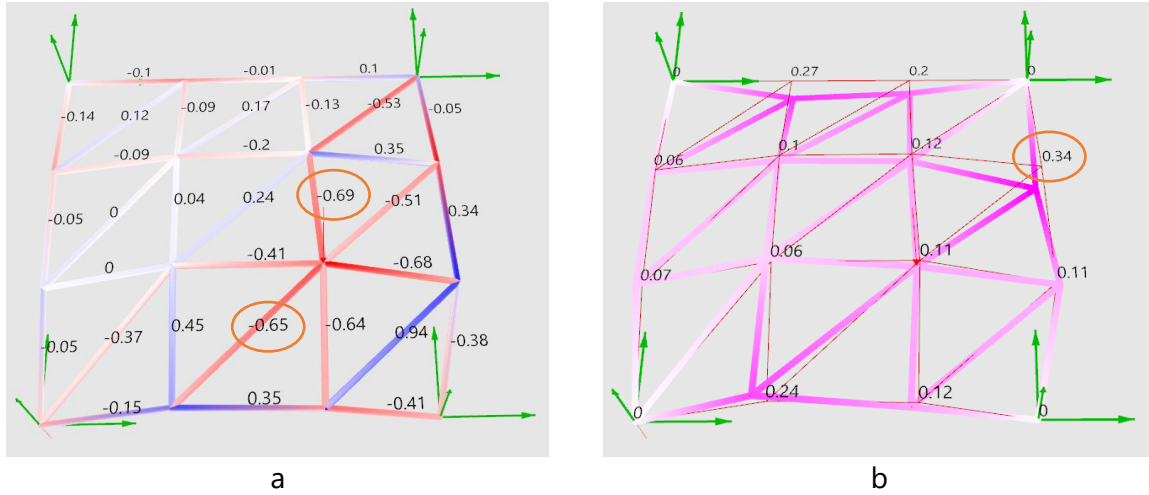
A more extensive analysis of global modes of buckling and local buckling is essential for this type of structure. Although not in the current scope of this study, these requirements are included in future works, Section 7.1.

Furthermore, local contacts and load transfer to the hub are also important. Different loading conditions should be conducted. Loading conditions include axial loading on the printed parts, axial loading with eccentricity, and axial loading with bending moment. Detailed finite element models can inform rigidity of the connection and load transfer characteristics.

## 4.7    Normal vectors of mesh vertices

The hubs are extruded along an axial line, called the hub axis. The hub axis is to be positioned in alignment with the normal vectors of the previously generated mesh. While verifying this previously generated mesh it was realized that the normal vectors on a cylinder were not aligned in the plane of symmetry as it was first expected. This is represented in Figure 30, where the perspective view (Figure 30a) shows the discretization and the front view (Figure

30b) shows the symmetry of the half cylinder and a zoomed view of normal vectors that are aligned. When the discretization is triangulated (Figure 30c) and the front symmetric view is zoomed in (Figure 30d) it is clear the normal vectors do not align anymore.



*a*

*b*

*c*

*d*
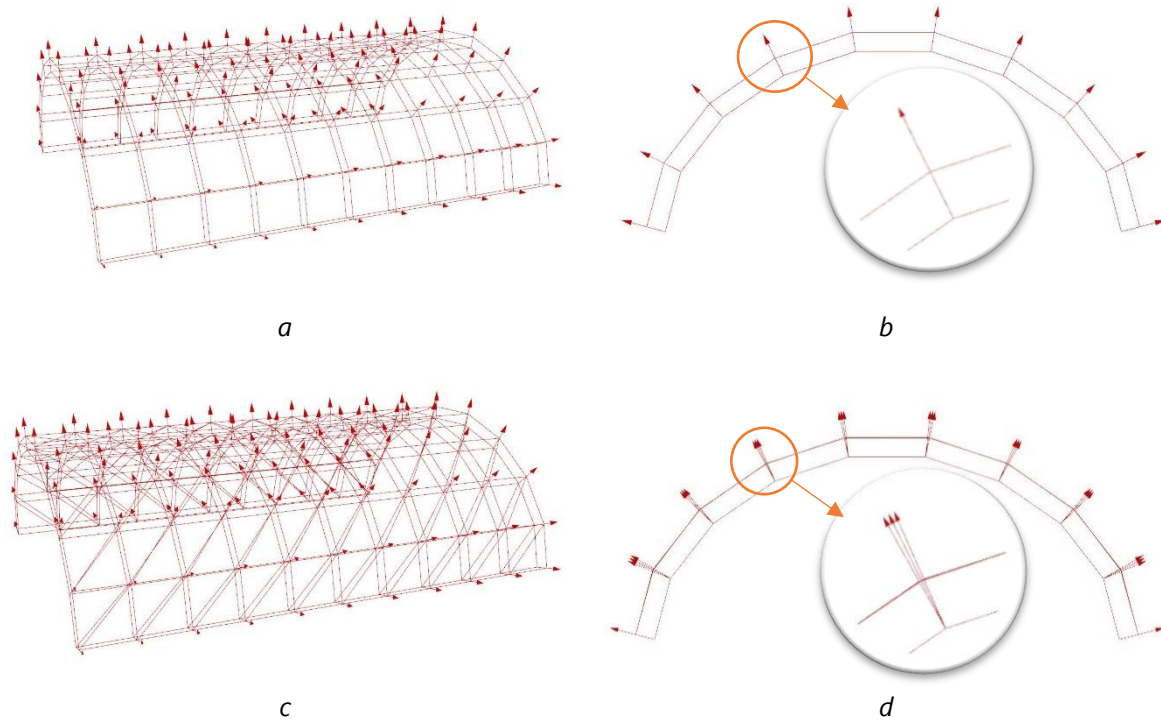
*Figure 30: Normal vectors on cylindrical mesh: (a) perspective view of quad mesh; (b) front view of symmetry and zoomed aligned normal vectors; (c) perspective view of triangulated mesh; (d) front view of symmetry and zoomed unaligned normal vectors.*

As it turns out the program calculates mesh vertices normal vectors through the average of the adjacent face normal vectors in respect to the area of each respective face area. The most accurate way of calculating this average would be to take into consideration the angle between adjacent edges of each face linked to each vertex. It is not done this way because the computational cost is higher. A simple way around this is to compute the normal vectors of the chosen surface prior to discretization with respect to the location of mesh vertices. As the differences produced are minimal, and the production of the pieces that will absorb such parameters do not rely on modularization, it was decided that the mesh offset would be applied through the normal vectors computed by the mesh normal vector calculator, and not the from the surface.

The meshes used for the physical model and the applications are built over NURBS surfaces, where $u$ and $v$ parameters are defined for discretization purposes. The built surfaces follow no particular rule, they are not specific parts of either spheres or cones. Extrusion for triangular

meshes are simply an offset of the vertices; and nodes present torsion, which is addressed shortly.

Here is another interesting concept that should be taken into consideration when creating surfaces for gridshells: there are three types of mesh extrusion, or mesh offset. The first is when vertices of the mesh are moved a constant chosen distance in the direction of the normal vectors of vertices. In this case, the faces and edges of the upper and lower layers of the mesh may not be at constant distances from each other. This means that the cross-section of a tube might not be of constant height throughout the length of each edge of the mesh. Quadrangular and hexagonal meshes have properties that can allow for optimizations that take that particularity into consideration. Certain types of surfaces allow for edge offsets, which is the second type of offset, that allows for the constant cross-section. Face offset is the third type. In planar face meshes, if this type of offset is possible, then the two meshes are called parallel meshes. These concepts are all introduced and explored in detail by Pottmann et al. (2007). These authors continuously explore relations of discrete differential geometry and design that makes complex architectural surfaces into more feasible projects. The study of these relationships is often referred to as *fabrication aware design*.

## 4.8   Data structure

The way the data is organized in the program is key to create geometry for elements that depend on the position of other elements in space. One of the inputs for the cluster that generates the geometry of the interconnecting parts is a list of the bar centerlines. To generate this list of lines from the given mesh the following steps are taken. First, the mesh (either upper or lower layer) is decomposed into its edges and vertices. Then, a sphere is created centered in each vertex. The radiuses of the spheres are set to a fraction of the smallest length of the edge of the given mesh. A component allows for computation of the intersection of the sphere geometry with the geometries of the lines, outputting the portion of the lines inside the sphere. Figure 31a shows the extraction of these lines and the order of nodes in the mesh. Figure 31b presents not only the node identifiers (preceded by 'n') but also the bar identifiers (between curly brackets). This example is based on the produced physical model, presented in Section 5.1.
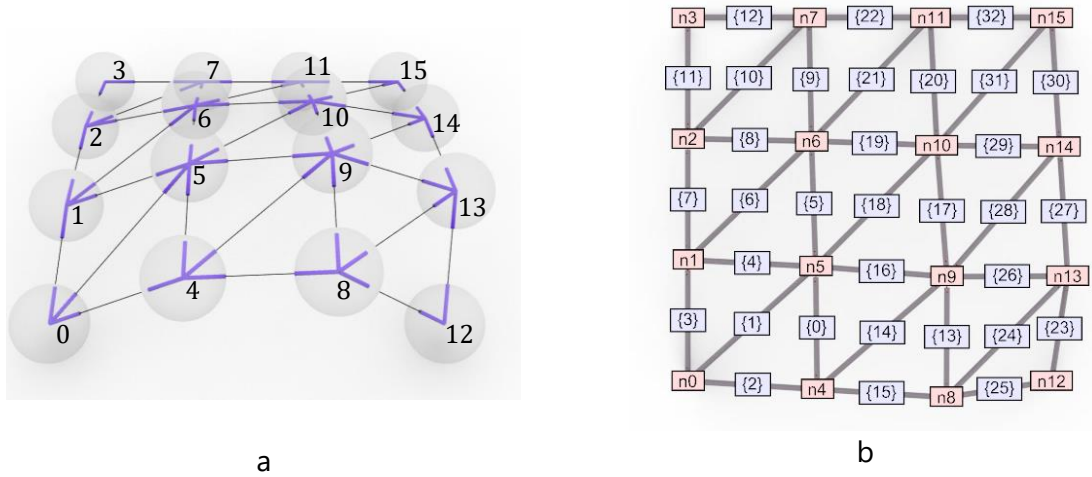
a          b

*Figure 31: Data structure in the model: (a): extraction of bar centerlines segments according to vertex; (b): numbered nodes and lines*

The segments of the mesh lines are grouped by vertex, producing a list of lists (also called a "tree"). Each sublist (or "branch") can have a different number of items. For instance, a vertex may have three lines arriving at it, while the next vertex of the list may have six. This data structure – lines grouped by vertex – quickly shows how many bars are connected to a node. Each item has its identification (Id) number in the initial data structure. Table 1 starts, from the top left, showing tree branches with one item each; the first numbers (A) inside curly brackets are the node identifiers, and the second numbers (B) are the line identifiers. These identifiers can be compared to Figure 31. Note that the second number (B) is not sequential, and they appear two times in the tree, representing the beginning and the end of the same line. The interconnecting parts are created using a point that is taken from each line segment. The data structure of these points sometimes relates to the mesh center points, and sometimes relates to the bar center lines. In Table 1, on the bottom, there are two data structures for the points.

*Table 1: Data structure for lines and points. A represents vertex Id; B represents line Id; (_,_,_) represents a point coordinate in 3D space.*

| Line tree $\{A;\ B\}$ | | | | Line tree grouped by point $\{A\}$ | | | |
|---|---|---|---|---|---|---|---|
| {0;1} | {1;3} | ... | {15;30} | {0} | {1} | ... | {15} |
| 0. Line | 0. Line | | 0. Line | 0. Line | 0. Line | | 0. Line |
| {0;2} | {1;4} | | {15;31} | 1. Line | 1. Line | | 1. Line |
| 0. Line | 0. Line | | 0. Line | 2. Line | 2. Line | | 2. Line |
| {0;3} | {1;6} | | {15;32} | | 3. Line | | |
| 0. Line | 0. Line | | 0. Line | | | | |
| | {1;7} | | | | | | |
| | 0. Line | | | | | | |

| Point tree grouped by line $\{B\}$ | | | | Point tree unflattened $\{B;\ A\}$ | | | |
|---|---|---|---|---|---|---|---|
| {0} | {1} | ... | {32} | {0;4} | {1;0} | ... | {32;11} |
| 0. (_,_,_) | 0. (_,_,_) | | 0. (_,_,_) | 0. (_,_,_) | 0. (_,_,_) | | 0. (_,_,_) |

| 1.(_,_,_) | 1.(_,_,_) | | 1.(_,_,_) | {0;5} | {1;5} | | {32;15} |
|-----------|-----------|---|-----------|-------|-------|---|---------|
| | | | | 0. (_,_,_) | 0. (_,_,_) | | 0. (_,_,_) |

Note that point Ids and line Ids correspond to connectivity matrix, used in Finite Elements Method.

A flattened tree can lose Id information of its elements, but an unflattening component can be used to restore that data. A tree previously used in the program workflow can be used to guide this procedure. In the given example there are 16 points and 33 lines; if the start and end of lines are considered, then there are references for 66 line segments and points Ids. The 66 line segments Ids indicate a total of 66 interconnecting parts to be printed.

Another component used is the duplication of elements in a list according to the length of other lists. This is needed when a measurement of one element is taken in relation to many other elements.

Short Python scripts are also eventually used for quicker computations with repetitive data. Loops and counters help extract and compute some information efficiently.

## 4.9   Twist angle

The twist angle is the angle between one normal vector of one hub in relation to the other connected to the same bar. There is one twist angle related to every bar. To calculate this, the data is organized in vertices grouped by line. Each line with node 0 and node 1. Each node has a normal vector previously generated through the mesh offset, as observed in Figure 32a, in the zoomed circle. Normal vectors of nodes are named $h_i$, $i$ ranging from 0 to the number of nodes in the mesh. For node 0 (Figure 32a), the normal is $h_0$, where the endpoint is node 3; for node 1 the normal is $h_1$, and the endpoint is node 2. Bar direction vectors are named $b_k$, $k$ ranging from 0 to the number of bars in the mesh. The centerline of the bar selected is $b_0$. A plane perpendicular to $b_0$ is created (Figure 32b). The twist angle is calculated through a center point, which is node 0 in this case, and two projected points on the created plane. Node 2 is projected on the created plane; this new projected point is called node $2_{proj}$. The same happens with node 3; the projected point is called node $3_{proj}$. In Figure 32b it seems as if node 3 and $3_{proj}$ are the same. However, Figure 32c shows an example where these projections do not lead to the same location, i.e., when the hub's normal is not contained in the created plane. Then,

the smallest angle between node $2_{proj}$ and node $3_{proj}$, with node 0 as the center point is calculated. In Figure 32b this angle is 5.5 degrees, while in Figure 32c this angle is 13.7 degrees. Figure 32c shows bar number 26 ($b_{26}$) of the physical model built.

For easier fabrication, it is specified that the bars be perforated with aligning holes. It would be unpractical to measure the twist angle to drill the holes in the correct angles for each individual bar, which already have different lengths, in the laboratory. Since the production of the interconnecting parts is through 3D printing, this parameter is included in the production of such parts. Thus, the angle correction is made always at the interconnecting part corresponding to node 0 of each bar, in such a way that the holes are aligned. The pinhole detail and screws can be observed in Figure 24, at the beginning of Section 4.4.
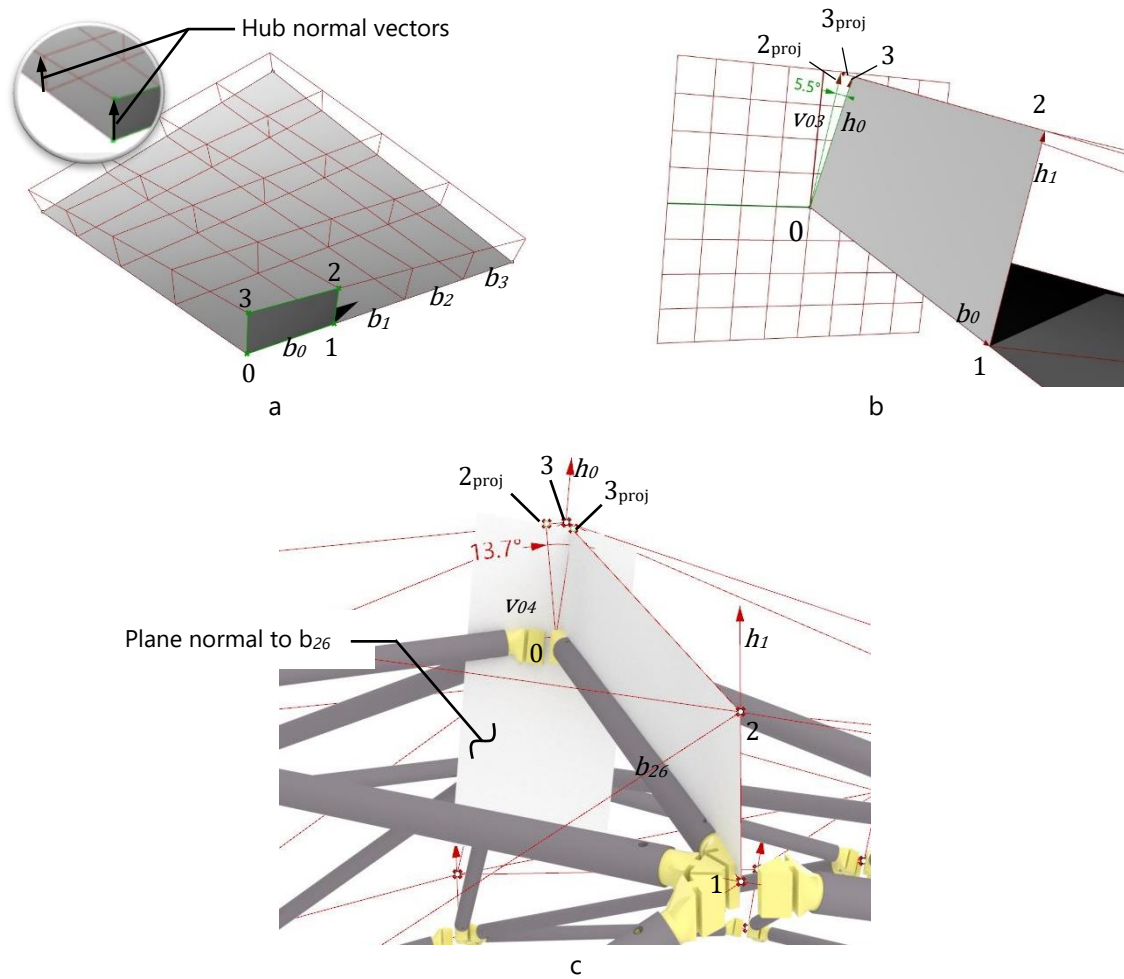


*Figure 32: Twist angle measurement: (a) numbered elements in global view; (b) numbered elements in local view, small twist angle; (c) numbered elements in local view with visible bars and interconnecting parts, larger twist angle.*

## 4.10  Adjacency angle

The adjacency angle is defined as the angle between the bars projected on the plane normal to each hub axis vector (Figure 22).

The chosen hub for the proof of concept model has eight possible notches for connections of bars. These notches are evenly distributed at 45-degree angles between one another, radially, in the hub. The ideal mesh for such a node would consist of polygons with adjacency angles of 45 degrees or multiples. The exact angle seldom happens in real-world applications, so the mesh should be designed to have adjacency angles as close as possible to that defined by the chosen hub. The interconnecting printed parts absorb the small distortion where angles are not exact multiples of 45 degrees. Some meshes may benefit from allowing more types of hubs with different angles between notches. However, some adjustments for the interconnecting parts may be needed — the next section details how to best position the hub to minimize these adjustments.

Figure 33 shows an example where bar vectors are $b_k$, $k$ ranging from 0 to 5, and the vectors of the bars projected onto the plane normal to the hub are $bp_k$. It is possible to observe, in this image: the hub and its normal vector; the plane created normal to this hub; the bar centerlines; the vectors in the direction of the bar centerlines; projection vectors; and the projection of bar vectors on the defined plane. The angle in question is highlighted in a circle.
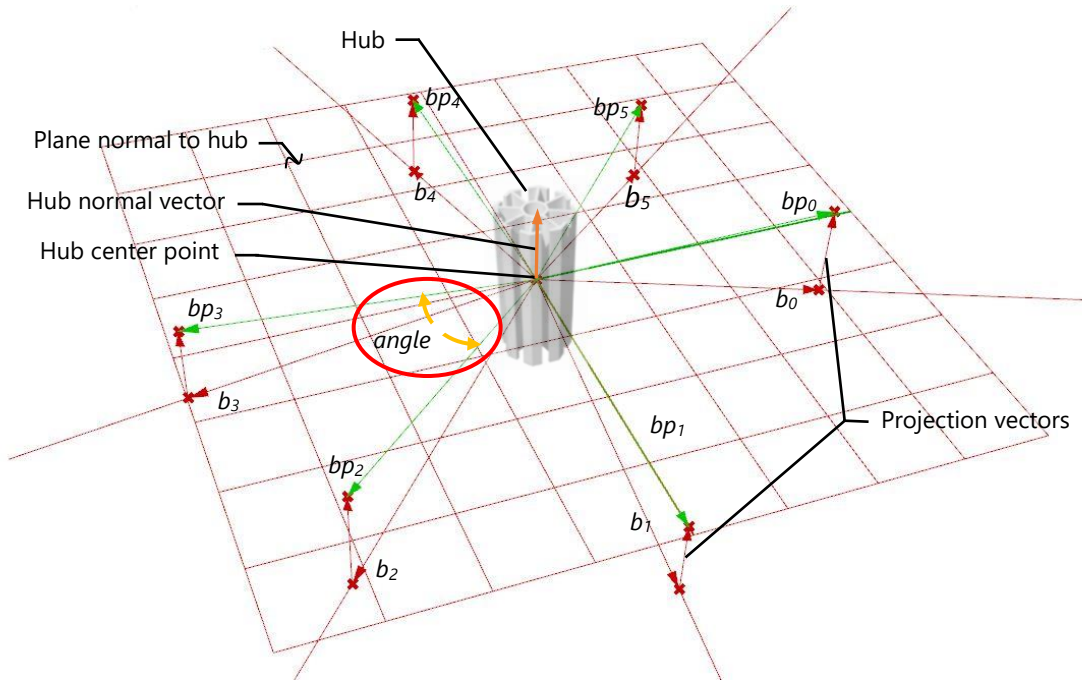
*Figure 33: Projection of bar vectors on the plane normal to the hub. Highlighted in a circle is the angle between bars measured in the plane normal to the hub normal vector.*

The mesh should be generated in such a way that these projected angles are as close as possible to 45 degrees or multiples; this way, there will not be the problem of two bars overlapping in the same notch. This leads to the conclusion that the interconnecting printed parts absorb a 'distorted angle' tolerance where angles are not exact multiples of 45 degrees between bars. Since this may be the case on most connections for the unconventional surfaces, it is ideal that these distortions be the least possible. The intention is, then, to position the hubs in space in such a way that these parts will have the least number of distorted angles, and that these angles be the smallest possible. The way this is presently handled includes 'introduced geometric imperfections' throughout the structure. Some meshes may benefit from allowing more types of hubs with different angles between notches, however, some adjustments are probably still needed. The next section details how to best position the hub to minimize these distortions.

## 4.11 Hub rotation to minimize distortions

Each hub has a normal vector ($h_i$, $i$ ranging from 0 to the number of nodes in the mesh). On the plane normal to the hub vector, eight vectors ($s_{ji}$, $j$ ranging from 0 to 7) are produced radially with 45-degree angles between each other. The number of notches ($j$) can be changed

for any other given number. For instance, if hubs of six notches are chosen, then six vectors are produced ($j$ ranging from 0 to 5) spaced radially at a 60-degree angle. To create the polar array of notch vectors, first, one must be positioned correctly in space. The notch vector 0 ($s_0$) is aligned with the projected bar centerline 0 ($bp_0$) (Figure 34a). Centerline 0 is not any particularly chosen line, it solely depends on the database created by the program. The database is organized with centerlines grouped by node. After the alignment between the first notch vector and the first projected bar vector, the following notch vectors are created (Figure 34b).
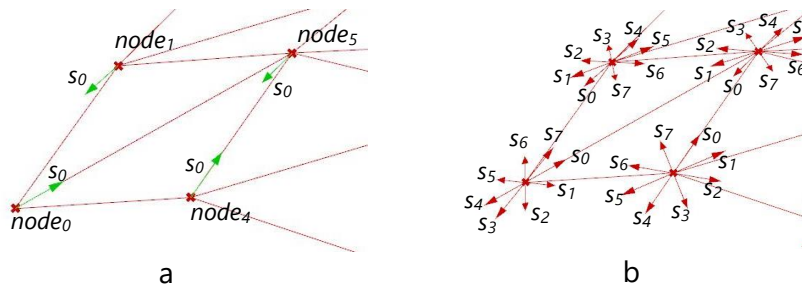


Figure 34: (a) positioning of the first notch vector aligned with the first line of each point, projected on the plane normal the hub; (b) array of notch vectors starting from the first positioned vector.

Then, the angles between the first notch vector and each projected bar vector are calculated. Any other angle needed for the choice of notch vector can be inferred from this measurement. Yet, the creation of all the notch vectors aids further programmed steps. Following is a description for a generic type of hub, and next, examples are presented.

The angle between two adjacent notches is $\alpha$. The angle between an arbitrarily projected bar vector and an arbitrarily chosen notch is $\beta$. The maximum angle between any projected bar and its closest notch vector is half of $\alpha$. Hence, $\beta$ can be reduced to an interval of $-\alpha/2$ to $\alpha/2$. If $\beta$ is not already in that interval, subtract $\alpha$ to $\beta$ until it is in that interval. The number of times the subtraction is computed corresponds to the identification number of the vector closer to the bar. This property is given by construction of the polar array of the notch vectors. The notch vector closer to each bar needs only to be chosen by its identification number, and this is the purpose of previously creating the array.

The calculated $\beta$ angles (within the interval of $-\alpha/2$ to $\alpha/2$) are now used to compute the correction angle for rotation of the hub. Although the $\beta$ angles are already computed, another way to compute them is described following. Examples are given below in order to conclude how to best evaluate the correction angle.

The β angles can all be measured from bar to notch; counter-clockwise is considered positive. The smallest β value (βₛ) is added to the largest β value (β_L) for one given hub, taking into consideration the positive and negative signs. Note that the smallest value of β may be the largest negative angle. The correction angle is the average between βₛ and β_L. Then, the notch positions are all rotated in the direction of the correction angle. Consequently, the modulus of the largest angle between notches and bars will be smaller than the largest angle computed before the correction. This way, most bars are slightly out of alignment in relation to the notch, but none is extremely off while the others are perfectly aligned. This way, the "introduced geometric imperfection" is distributed throughout the structure, without one very distorted angle weighing off the balance.

An example of angle measurements with three bars (numbered 0, 1 and 2) and a hub with eight notches (α=45°) is presented in Figure 35. This figure shows the placement of the first notch vector aligned with the first line (line 0). The angles between that vector and all the bars in that node are measured in relation to the plane normal to the hub. The angle for bar 0 is 0 degrees by definition. The angle for bar 1 is 29.89 degrees, and for bar 2 it is 260.92 degrees, measured from bar to notch, following counter-clockwise direction. From this measurement, only, it is possible to calculate all other angles required, since notch vectors are at a constant angular distance.
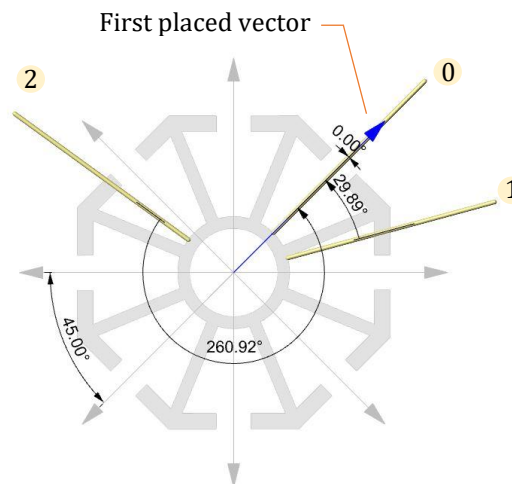


*Figure 35: Angle measurement from bar to notch.*

The choice of calculation for the best angle to rotate the hub can be exemplified in three cases. The first is presented in Figure 36a, where one notch is aligned with one bar (0.00°), one notch is 15.11 degrees clockwise (-15.11°) from bar 1, and the other notch is 9.08 degrees clockwise (-9.08°) from bar 2. The smallest value is -15.11, and the largest value is 0, if both are added

and divided by 2, the result is -7.555. If the hub is rotated the opposite direction, counter-clockwise, by 7.555 degrees then the distortion is well distributed among the bars, as shows Figure 36b. The second case is the exact opposite of the first, where the angles are all positive in relation to the closest notch. The smallest number is 0 and the largest is a positive number, depending on the angles measured. Then the rotation is given by 0 added to the second number (a positive value), and the sum of both values is divided by two. The result of that calculation is the adjustment angle to be applied to the hub, the rotation is clockwise. The third case is presented in Figure 36c, where some of the angles are negative and some are positive. The calculation, however, is still based on the same principle. The smallest value, in this example, is -15.11, the largest is 9.08. Both values are added, and the sum is divided by two, resulting in -3.6. The rotation for the hub is, then, then, in the opposite direction, counter-clockwise, of 3.6 degrees, as shown in Figure 36d.
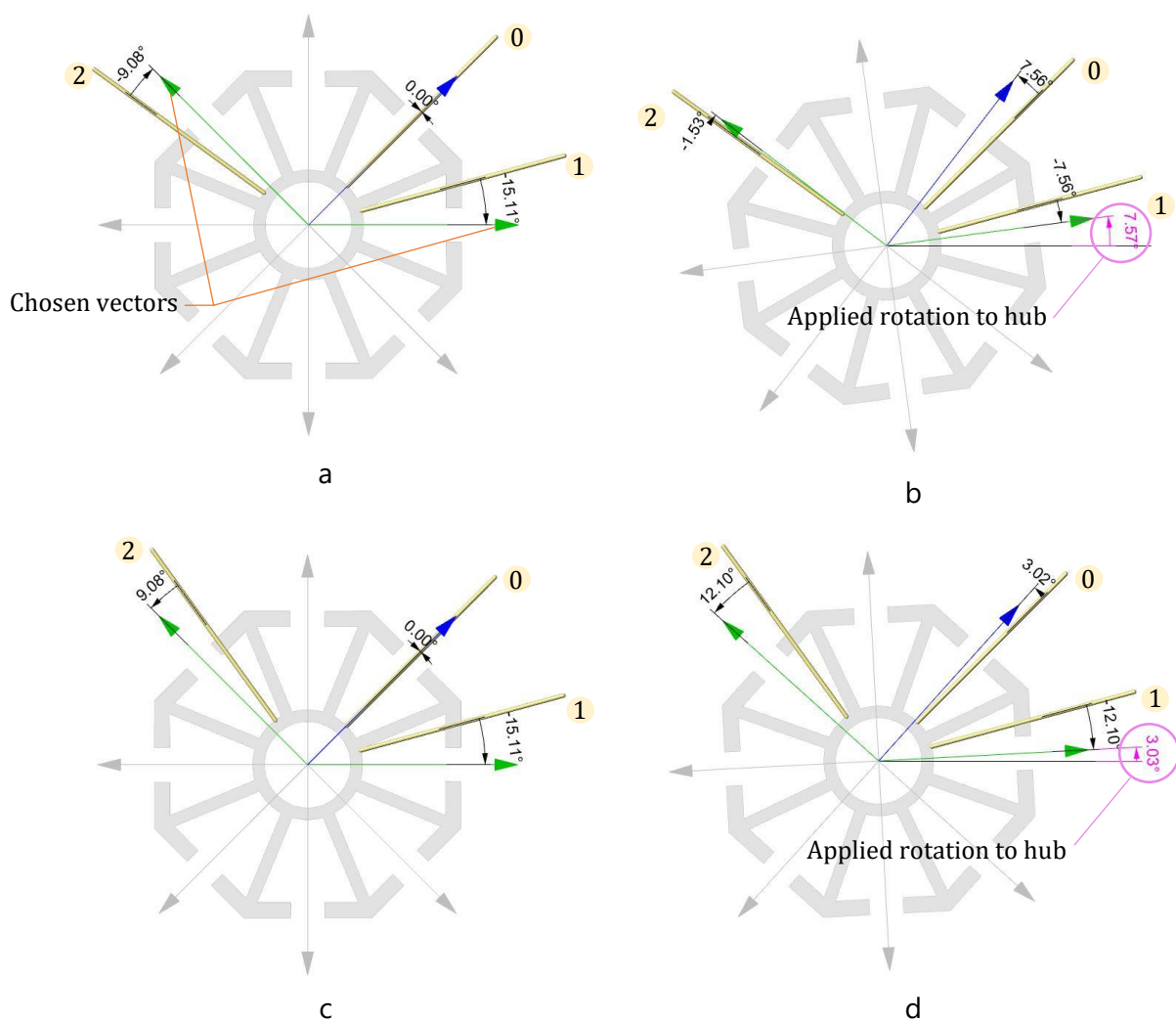


Figure 36: Angle measurements for hub rotation: (a) case 1, all angles in one direction; (b) case 1 solution; (c) case 2, angles in both directions; (d) case 2 solution.

These cases all consider a previously well-defined mesh with consistent angles between bars and chosen hub types, as mentioned before.

The same procedure can be realized automatically for any other hub with a different number of notches. If a structure can have hubs of 8 or 6 notches, then the choice between one or another is given by the smallest average of angles (in modulus) between notches and bars of the node – after the hub rotation adjustment. There are, currently, three choices of nodes available in the programmed parametric description. The number of notches can be chosen by the user; it is currently set to 5, 6 and 8. Adding more options of hubs is of no extra complexity, however, the implementation may not be the most efficient, thus, more time for computation should be allowed, especially if there is a large number of nodes and bars in a given structure.

Although this feature is called out as an introduced geometric imperfection, the axial load from the tubes are still intersecting at one point. It is the way the contacts between the interconnecting parts and the hub happen that will determine how these adjustments influence load transfer. This would require a detailed finite element analysis for various cases, which is not in the current scope of this work.

## 4.12  Adjusting the geometry of the interconnecting parts

Previous images of interconnecting parts were created with perfectly aligned angles. For other meshes, the adjustment needs to be implemented still. With the hub rotated to the best possible position, the interconnecting parts must be updated. Figure 37a shows where adjustment is required, the small gaps are circled in the image. To change this geometry the interconnecting part is divided into three subparts: subpart A of the geometry is generated according to notch location; subpart C is generated according to bar location; and subpart B connects A to C. Figure 37b shows these subparts.
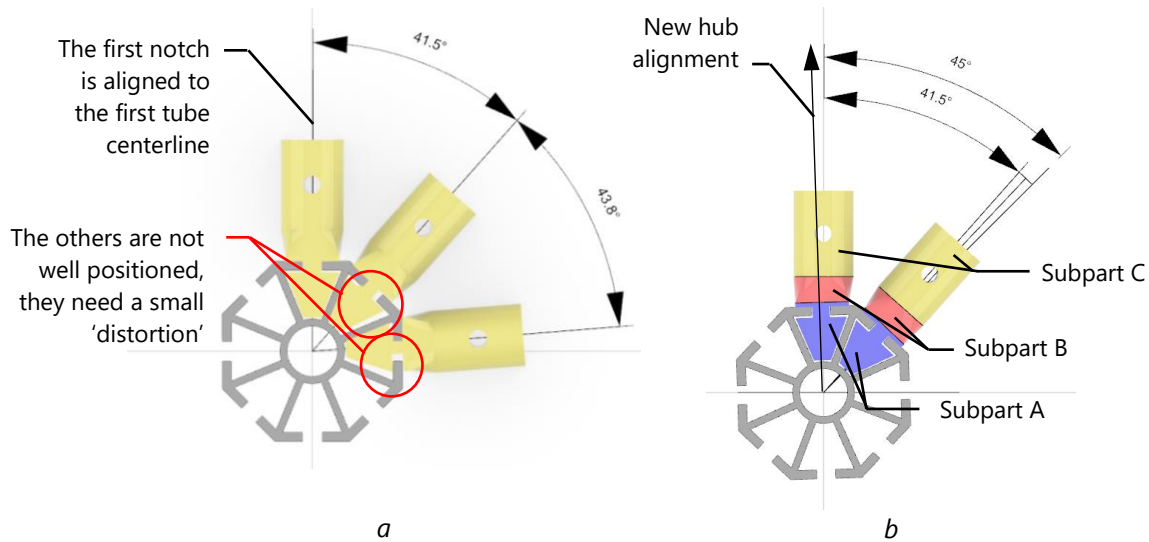
*Figure 37: Interconnecting parts: (a) parts requiring adjustments; (b) separated subparts and the parts adjusted.*

## 4.13  Generation of subpart C

The subparts C are generated from the segments of mesh lines depicted in Figure 31a. Subpart C is a pipe with a predefined radius. The start point of the pipe is the intersection of the segments of mesh lines and the external cylinder (Figure 38). External and internal cylinders define a transition zone from subpart C to subpart A. The part between both cylinders is called subpart B. The radius of the internal cylinder is the same as the radius of the hub, and the radius of the external cylinder is larger than the internal one, by any amount considered necessary by the user. The pipe created at the defined intersection point is extended through a vector of any amplitude desired, in the direction of the bar centerline; it is called extension vector.
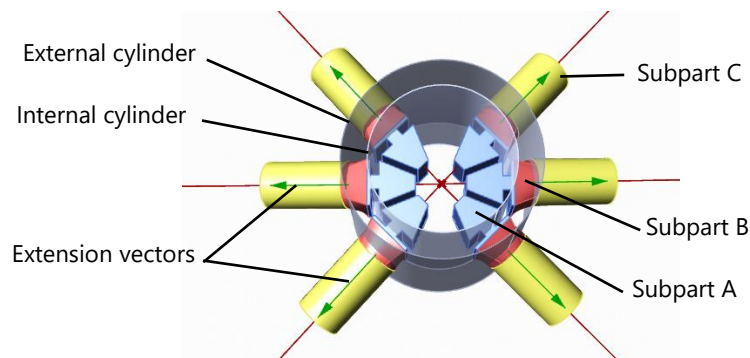


*Figure 38: Internal and external cylinder used as aids to create geometry; subparts; and extension vector.*

For the physical model presented in Section 5.1 the amplitude of the extension vector is set to 20 mm, the external cylinder radius is set to 27 mm, and the internal cylinder radius is set to 20 mm.

## 4.14  Generation of subpart A

The geometry of the hub notch is drawn into Rhino, and the lines representing the outline of one notch are inserted in parametric software (Figure 39a). This allows slight modifications to the notch geometry. The restriction is that only the control points of the curve can be changed, the curve itself should not be redrawn. If the curve is redrawn, then the programmed cluster of the local geometry generation will need adjustments. The direction of the original geometry is given by a vector represented as an arrow in Figure 39a.

After the notch outline is complete, a small offset is created to generate the outline of subpart A. The offset accounts for the needed gap to fit the printed part into the metallic hub. The "offseted" curve is translated (copied) to every location where the notch is needed. The origin for the translation is the original hub center point and direction vector (Figure 39a), and the destinations are the mesh center points with the directions of the corresponding chosen notch vectors (see Section 4.11). After this step, the planar notch curves are aligned to the correct direction (Figure 39b), but they are still not aligned to the correct hub normal plane. A rotation about the notch vector axis is completed, providing the final needed alignment (Figure 39c).
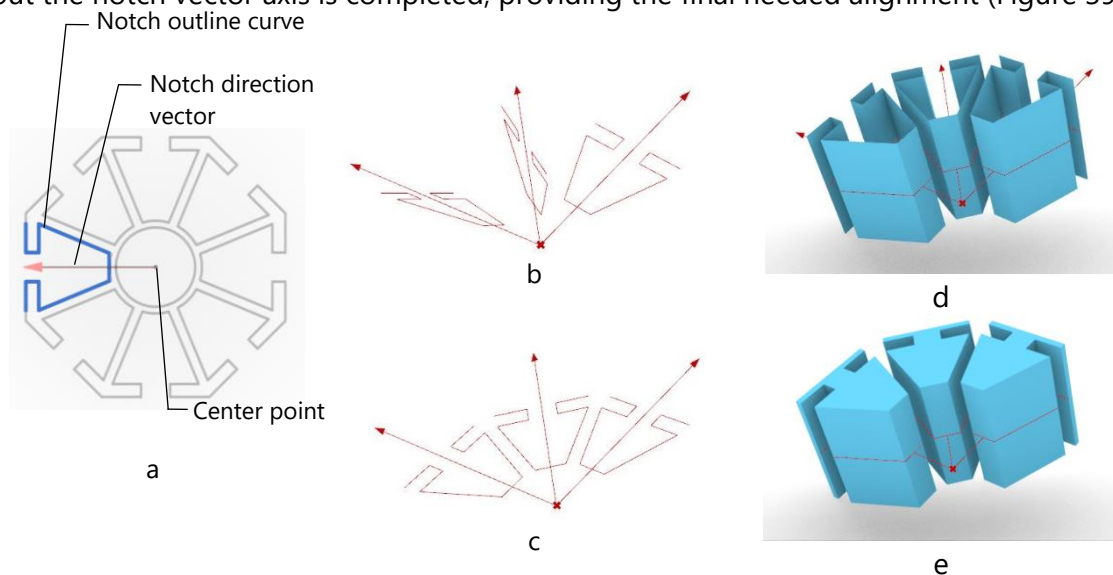


Figure 39: Subpart A: (a) outlining curve of the notch taken from the geometry of the hub; (b) notch geometry in the correct direction; (c) notch geometry on the correct orientation plane; (d) extrusion of notch geometry; and (e) subpart A complete.

Next, the curve is extruded to form the surface of subpart A (d). The hub vector guides the extrusion of the subparts related to the corresponding hub. The length is half of the intended height for the hub. The vector is reversed, and the same length is extruded in the opposite direction. This step is completed after the top and bottom surfaces join the geometry (Figure 39e).

## 4.15  Generation of subpart B

Subpart B joins a rectangular section from subpart A and a circular section from subpart C. If a surface is attempted to be created between both sections with current components, there are enormous chances that it will fail, or that a very twisted surface will be created. If the sections are simplified into segments of curves, however, the same components will perform perfectly. Subparts B have one-quarter of the surface created highlighted in Figure 40a. All quarters are joined into one surface, and then joined to subparts A and C (Figure 40b).
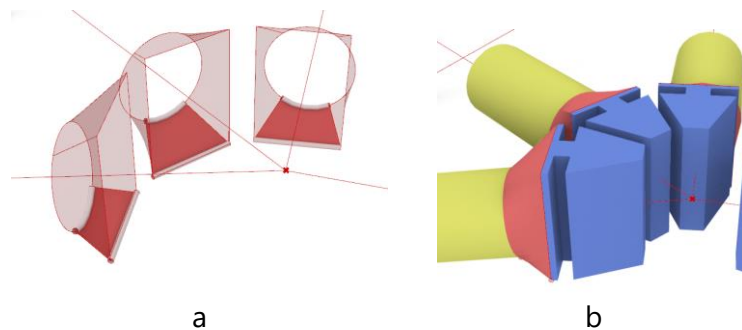


a                                b

*Figure 40: Subpart B with (a) a quarter of the surface highlighted, and then (b) united to the other geometries.*

## 4.16  Incidence angle: repositioning the connection center point

Mesh vertices provide the connection center points; mesh normal vectors provide the incidence angles for the bars. The incidence angle is defined as the angle between a bar and its corresponding hub normal vector. Consequently, there are two incidence angles for each bar. Figure 41a shows the incidence angles for two bar centerlines connected to one hub. Figure 41d shows the same centerlines; however, the hub normal vector is modified. It is possible to observe the influence of the incidence angle over the geometry of the interconnecting part. For both options, it is possible to note a significant discontinuity between subparts A and C. This discontinuity can be clearly observed when all the bars arrive at a center point from one side of the curvature of the surface. This is inferred after visual inspections of varying surfaces. The center of extrusion of subpart A should be modified to lessen this

discontinuity. A movement of the center point for that extrusion is, then, implemented. Figure 41b and Figure 41e show the difference between previous interconnecting part geometry and the resulting one, where the center point was modified. The resulting geometry is, then, observed in Figure 41c and Figure 41f.
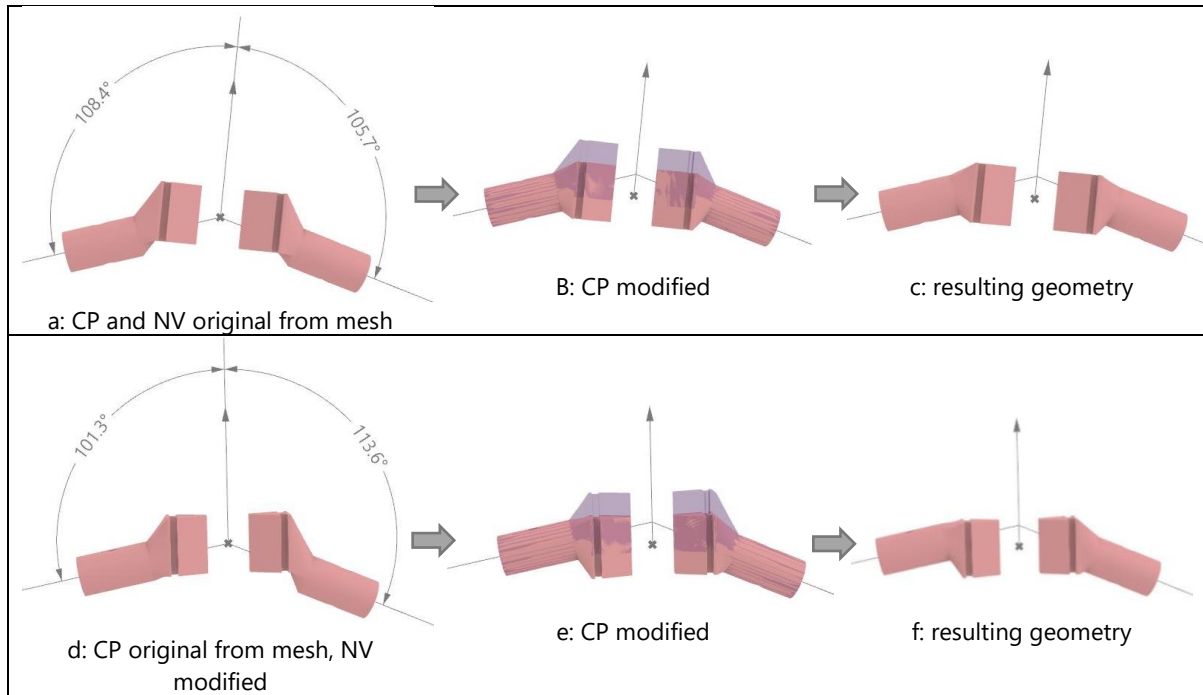


*Figure 41: Center point (CP) and normal vector (NV) are modified to show influence on local geometry of the interconnecting part.*

The modification of the normal vector here is applied only to show the influence of the incidence angle on the local geometry. The normal vector is given by the global generation of the mesh, and it is not modified for further applications.

To modify the center point for the extrusion of subpart A, the external cylinder intersection points with the lines, already described in section 4.13, are used here. Figure 42a shows the cylinder, the bar centerlines, and the intersection points. These intersection points are projected on the hub axis. Then, the average is taken of the collection of points projected on the hub. The average point is chosen as the new hub center point (indicated with the larger arrow in Figure 42a). This way, subpart A is generated in a better location with respect to most of the lines arriving at the hub. Figure 42b shows the modification of the geometries, where old and new positions are identified, as well as the mesh center point, that is substituted by the average point for the generation of subpart A.
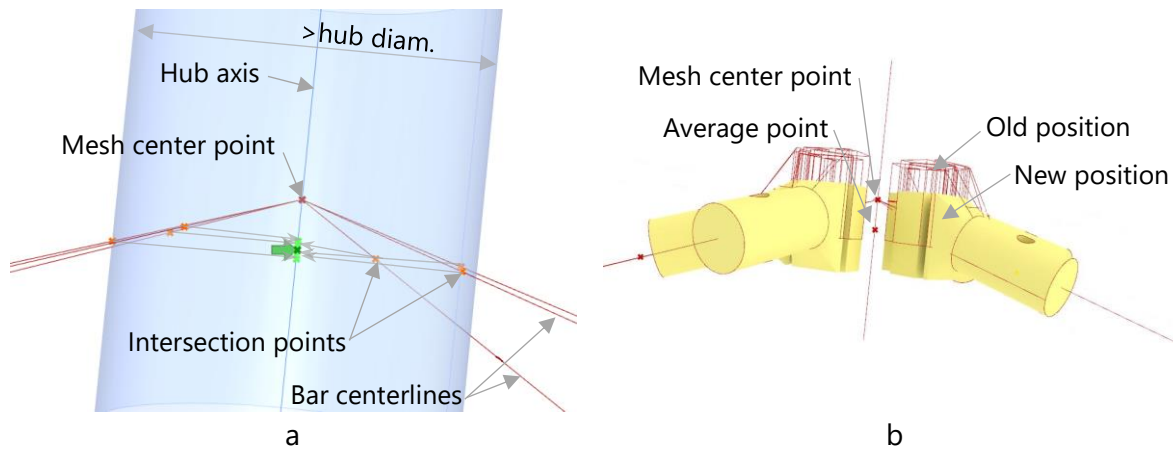
*Figure 42: Adjustment of the hub center point: (a) projection of intersection points on the hub axis; (b) result of this change.*

## 4.17 Fabrication tolerances

This section concentrates the adjustments implemented in the parametric definition that are defined by fabrication tolerances of machines used locally. The first adjustment corresponds to the length of each tube that is rounded to the nearest whole or half a centimeter. E.g.: a tube with 40.6 cm length is rounded to 40.5 cm, and a tube with 40.8 cm is rounded to 41.0 cm. This adjustment provides faster, and more precise cutting of the aluminum tubes chosen for the physical model. Additionally, the distance from the holes to the edges of the tubes should be the same for all tubes. This means adjusting the position of the holes in the printed parts towards the same alignment.

It would be reasonable to apply the adjustment of the length of the bar at the end of the program, only rounding up the numbers. However, the position of the pin holes, that now depend on the length of the bar, influence directly the geometry of the interconnecting parts. These adjustments are, then, made on the actual programmed geometry. Bar centerlines are kept their position at their midpoints, and their endpoints are altered. A vector with the amplitude of the desired distance for the pin holes is created and applied to those endpoints. The pin holes are, then, moved to the new locations using this vector.

The interconnecting parts to be printed also need tolerance adjustments to fit in the tubes and in the hubs, and for the screws to enter the pin holes. A tolerance value commonly used locally is an adjustment of 10% of the parameters. Subpart C diameter is reduced by 10% for it to fit in the tubes. The diameters of the pin holes, however, are increased 10%, for the screws to

pass through. These diameters are inserted as a varying number parameter in the parametric definition, and they are practical to change.

## 4.18 Tags

Tagging each element is critical for the correct construction of the physical model. For this project, the bars and the interconnecting parts need to be tagged, the remaining elements are all standardized and it is not necessary.

The tags of each of the parts to be 3D printed are their Ids. That consists of the node Id followed by the bar Id. These tags are generated through extruding the tag text and taking that solid from the original untagged piece (Figure 43a). The text entity does not allow for extrusion in the program, so a short script is included to take the outlining curves of each text. The tags in the cylindrical part of these elements are meant to be oriented the way the person assembling the model would read the numbers, horizontally, as Figure 43b shows. For the bars, a table of Ids is created. The information included in this tag is the Id of the bar, the length in millimeters, and the nodes it connects to (Figure 43c).



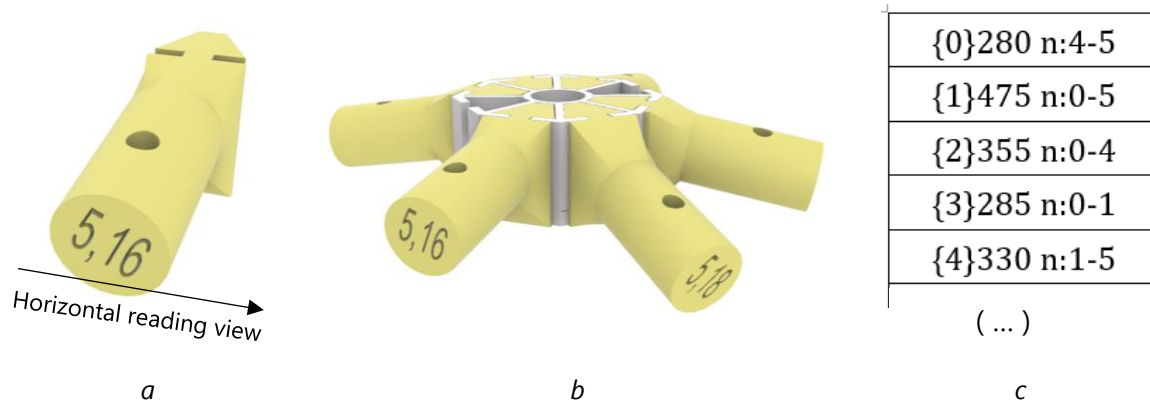| |
|---|
| {0}280 n:4-5 |
| {1}475 n:0-5 |
| {2}355 n:0-4 |
| {3}285 n:0-1 |
| {4}330 n:1-5 |
| ( ... ) |

Figure 43: Tags: (a) interconnecting part; (b) position in the hub, in such a way the builder can read the numbers; and (c) for the tubes.

The aluminum tubes are available in lengths of one meter and two meters. The intention of the bar tags is that they can be taped to the aluminum tube around the midpoint of each bar length. This way, the information of the length included in the aluminum tube can aid the process of cutting them, and later there should be no need of measuring each cut bar to identify which one it is.

Once the parts are printed, bar tags are in place, bars are cut and drilled, Figure 44 should be the only information needed to assemble the physical model.
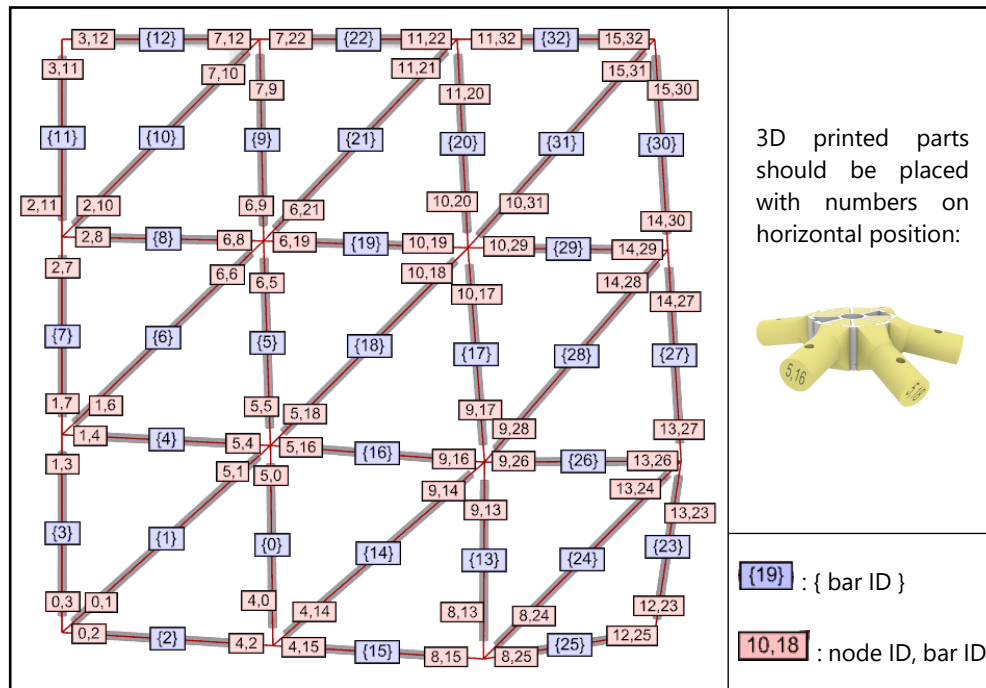
*Figure 44: Numbered elements for assembly*

There is no assembly sequence prepared to build the small-scale physical model. The experience of building this small-scale structure provides necessary insights for more complex models. The experience is described in Section 5.1.

# 5  Results

The parametric definition was reviewed, adjusted, eventual errors were found by visual inspection and through measurements, and they were corrected. It is possible to verify the angles between bars, the compensation of torsion angle in the pinhole, the compensation of machine tolerances through a proof of concept model.

The design presented in Section 4 was fabricated, and it is detailed in Section 5.1. The fabrication included the acquisition of material and working with different laboratories. The tubular bars were cut and drilled in the mechanical engineering laboratory. The interconnecting parts were printed in the mathematics and statistics institute's laboratory for digital fabrication. The tensile tests were conducted in the civil engineering laboratory.

The materials used for the model are not the ones intended for large scale fabrication, the connections were not dimensioned for best performance, and for these reasons the model is called 'proof of concept' – not 'prototype'. For a prototype, the future studies mentioned in Subsection 7.1 are crucial.

The same parametric definition was used to generate other computer modeling applications; they are presented in Section 5.2.

## 5.1  Proof of concept

An asymmetric surface was generated through Rhinoceros and imported into the parametric definition. The surface covers an area of 1m x 1m. The project to cut the bars was conducted to fit all the modeled bars in the least number of acquired bars with a length of 2 meters. Two aluminum tubular bars of 16mm diameter with the length of 1 meter had been previously acquired, leaving the need for five more bars of 2 meters. The project of the cut lengths of each bar, pin hole locations, and the hub profile was sent to the mechanical engineering laboratory for approval and execution. While the bars were sent to the laboratory, the parts to be printed were organized for the printer dimensions. Test pieces were first printed, and an adjustment to the size of the hole was executed. Then, a total of 66 pieces was sent to print in batches of 8 or 9 pieces. Although more pieces would fit in the printing space, it was recommended that fewer pieces should be sent for each batch. Printing errors can occur; therefore, the loss of time and material would be less if a smaller number of pieces were sent

to the printer at a time. There were four colors available for the material chosen and they were used to help the distribution of pieces at the time of assembly. The colors were distributed by quadrants, each being assigned to four hub locations. Figure 45 shows batches separated by printing area (15x15cm) and letters to differentiate each color group. Available colors were red (A), yellow (B), green (C) and blue (D). This step was created after contacting the team responsible for the printers.
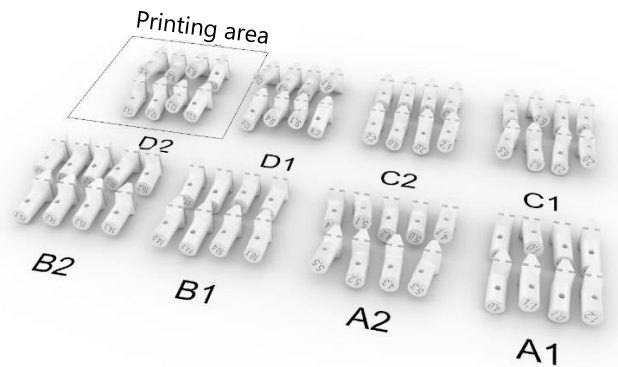


Figure 45: Organization of the printing process. Batches of eight or nine pieces were separated, each letter represents a color. The rectangle shows the available printing area.

Both polylactic acid (PLA) and acrylonitrile butadiene styrene (ABS) filaments were an option in the 3D printing laboratory. PLA is known to have higher tensile strength; however, it is brittle in collapse (3DHUBS 2019). Its chemical properties are poor; if exposed for a long time to the sun or rain it may start losing its original form. Although it is easier to print PLA with higher quality, it cannot be easily adjusted through abrasive methods such as electric sanders, as it melts, but a finer adjustment with hand files is possible. ABS is slightly tougher to print in higher quality, it requires a heated bed in order to avoid warping between layers, but, after printed, it can be smoothed with acetone, and it can be sanded down. It has a more ductile response under collapse; however, it has lower strength. The PLA was chosen for several reasons: the physical model will only be exposed in the protected environment inside a building; it is useless to foresee collapse (no need for ductility) since it will not be subjected to any safety tests; the PLA has higher strength than ABS.

PLA is commonly made of sugarcane or corn starch and its marketing suggests that it is biodegradable. However, it is biodegradable only in industrial composts with elevated temperatures and very specific conditions. In conventional landfills, the material takes just as many years as any other plastic to biodegrade. As industrial composts are extremely rare in

most cities another recommendation is available for disposal after use. The best way to treat plastic once it exists is to maintain it as plastic, using it wisely and recycling it (Filabot 2019). Fortunately, São Paulo has both industrial composts (Fragmaq 2017), and recycling facilities.

After the material is selected, other printing choices are conducted. The orientation of the piece on the printer is important for several reasons. First, the deposited layers of material produce a weaker plane of rupture, for this reason, the weaker part of the piece should be directed perpendicular to the deposit layers. Second, the best printing quality is reached when the layers are directly on top of the other, or smaller than the one before. When the following layer is larger the deposition of layers may get irregular. When this happens a support structure with less material and less density is created, it must be detached after printing. The orientations of the pieces must be so the part fitting in the hub (subpart A) has the best quality. This is achieved positioning this part in alignment with the plane of the printing bed, as shown in Figure 46.



*Figure 46: Interconnecting parts being printed.*

The parts were printed with 90% material density, which would take more than one hour less than printing 100% of material density for each batch of 8 to 9 pieces. The printer estimated a total of 4 hours and 30 minutes for the first batch; however, it took almost double that time to complete. The last batch of 8 pieces, all with the same parameters, took exactly 6 hours and 15 minutes to complete, instead of the initially estimated 3 hours.

As stated earlier, the choice of printing in batches of 8 or 9 pieces at a time was due to possible machine errors, and, thus, less loss of material if such an error occurred. Errors did occur, such as the printer stopping suddenly in the middle of the printing process for no apparent reason. Another error was not using enough glue on the printing bed, causing a piece to detach and clutter the printing process. Another error was due to lack of lubricant in machine gears, which caused the printer to shift over to the side approximately one millimeter. Eventually, another

machine, which was being used for another project, was made available to continue printing the pieces from this project, and such errors came to an end. Fortunately, the described errors were all fixed in the previous machine, and it was used again for the last batches.

The printed parts are shown in Figure 47a only to exemplify the difference in angles in the pin holes. It also shows that the tagging was printed with good resolution. Figure 47b shows how the color was used to accelerate the assembly process. If all pieces had been the same color it would have taken more time to separate the parts to their corresponding node locations.



| a | b |

*Figure 47: Interconnecting printed parts: (a) test of the fitting between parts; (b) distribution according to colors.*

The model was built in less than one hour, from separating the material to tying the last screw. If the parts were to be attached to the tubes prior to the assembly process, then the time on-site would lower considerably.

The single sheet of paper with bar and interconnecting parts information was enough to build the model correctly. However, the interconnecting parts, that were already fixated to the last hub, were taken from the hub so they could be first fitted into the bar. It was, then, easier to fit the piece in the hub. This experience provided insights to assembly sequence and tagging information, presented in Section 6.

Figure 48a shows the side view of the completed model, other views can be observed in Figure 48b and Figure 48c. It proves the programmed definition works, and the structural system is viable for small scale with the given fabrication process. Connection details are shown from above (Figure 48d) and from below (Figure 48e). Ideally, screws with the exact size of the diameter and color of the tubular bars of the aluminum would have been chosen if available.
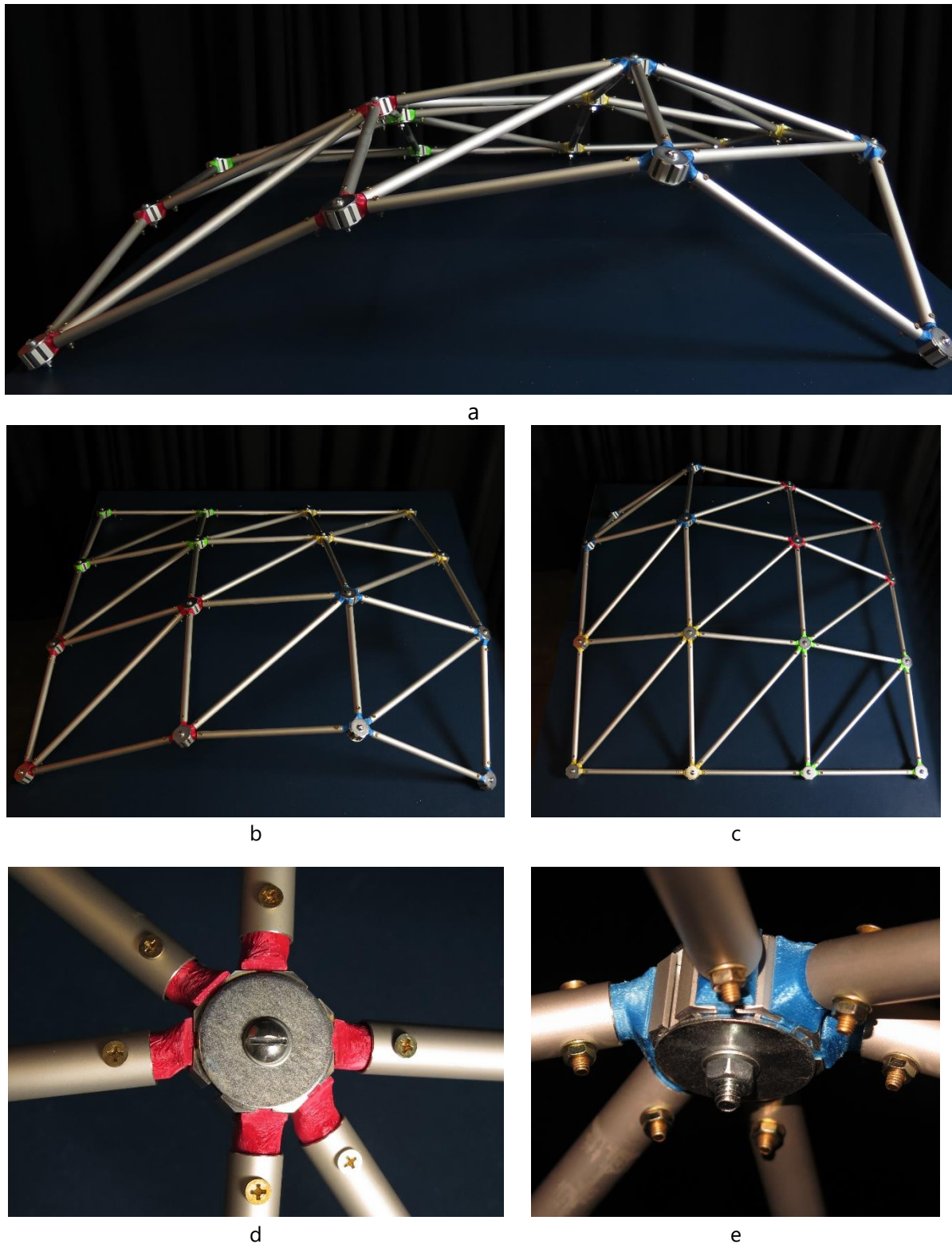
*Figure 48: Physical model: (a, b, c) global views; (d) connection from above; (e) connection from below.*

Two tensile tests were conducted. The first test was the tensile properties of the printed plastic, following the ASTM D638 test for Type I plastics (ASTM Standard D 638 -02a 2003). The test piece was printed with the same specifications and material as the printed pieces used for the

physical model. The second test was for the tensile strength of the bar-screw-printed piece-hub connection.

Figure 49a shows the test piece ruptured, and, although the global aspect of test 5 is failure by shear, it is not the case when seen in detail (Figure 49b). The 3D printer was set to print in diagonal lines; the tensile strength of the diagonal lines was reached and the 'fibers' were ruptured in the normal direction locally, although globally it looks as if it were ruptured diagonally. The 'fibers' can be more clearly distinguished in Figure 24c.
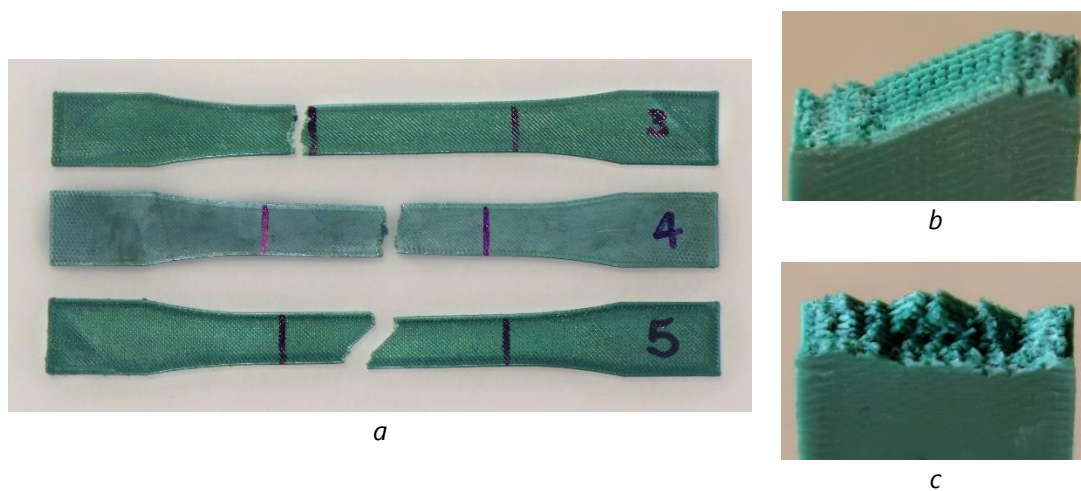


*Figure 49: Tensile tests: (a) global view; (b and c) local view.*

The tensile strength of the PLA printed with diagonal lines and 90% density is of 26.4 MPa. The first two test pieces were discarded because of measuring errors from the tensile test machine. The results can be observed in Figure 50.
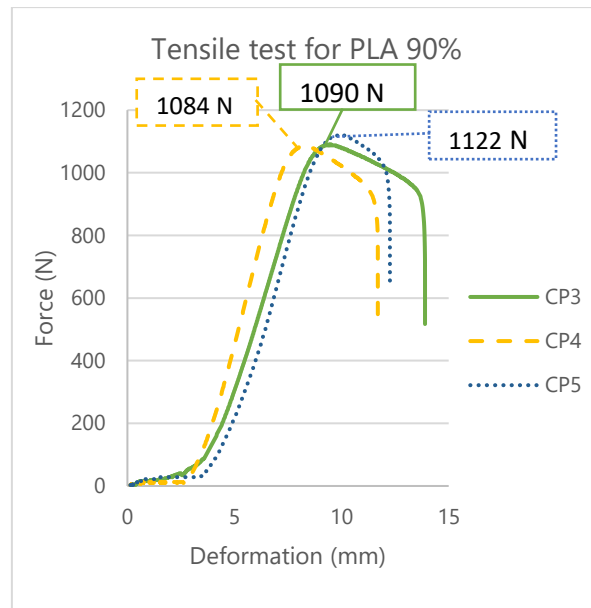
*Figure 50: Graph: PLA diagonal printing with 90% density tensile test.*

The tensile test of the connection is shown in Figure 51a. The printed PLA piece was ruptured around the screw location, as shown in Figure 51b. The calculated area of PLA in the screw section is 81.56mm$^2$, while on the thin part that connects to the hub it is 81.49mm$^2$. This tensile test result is discussed in Section 6. Figure 51c shows deformation on the screw, where the straight line gives a reference and the slight deformation can be seen more clearly. Figure 51d shows deformation on the tube at the location of the pinhole; the circle on the side can be used to compare the forms.
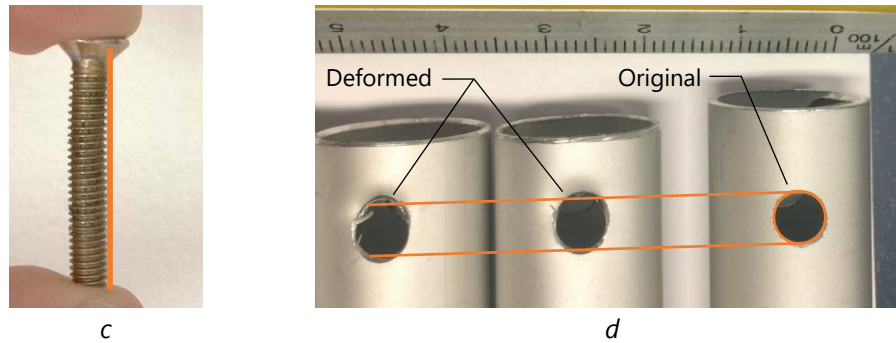


*a*



*b*

*Figure 51: Tensile test of the connection: (a) how the connection was tested in the machine; (b) ruptured connection; (c) deformation on the screw; (d) deformation on the tube.*

Three connections were prepared for the tensile test. The results can be observed in Figure 52.
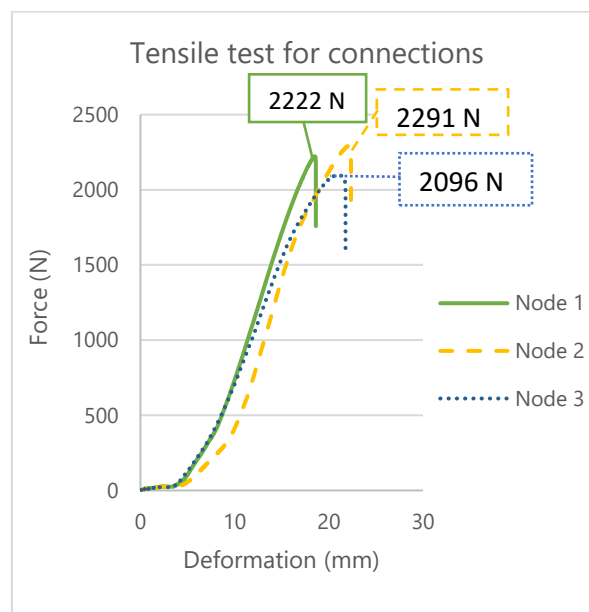


*Figure 52: Tensile tests for the connection.*

## 5.2  Applications

In addition to the physical model that was produced to provide proof of the concept developed in the computational environment, further explorations of meshes and forms are also conducted. Three applications are presented here: a geodesic dome; an inflated curved surface; and a wave-like surface. Each application has a different purpose, which is detailed in the corresponding sections.

### 5.2.1  Geodesic dome

The geodesic structure is widely used for small to large scale applications, hence, it is essential to apply the developed system to this iconic type of structure. Additionally, the hub choice

part of the program can be verified, since this mesh produces a well-known result. A geodesic sphere is created and a plane parallel to the horizon at an arbitrary height cuts the shape of the sphere. The scale of this dome is larger than the prototype, consequently, the notch geometry is scaled and the numbers defining the geometry of the connection are also changed. Next, the mesh is inserted in the parametric definition for the connection and the geometries are automatically computed. Some parameter adjustments of the connections are needed and, finally, Figure 53 shows the result of this application. Figure 53a is the top view of the dome, Figure 53b is the perspective view of the dome, and Figure 53c shows the interconnecting pieces distributed on the horizontal plane for fabrication.
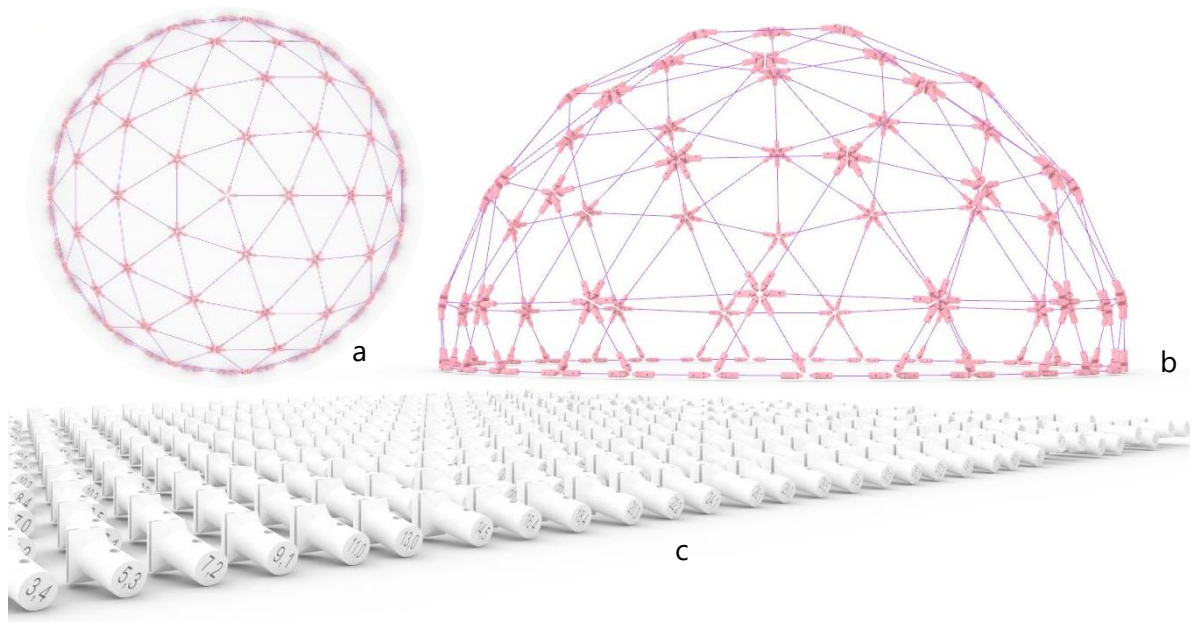


*Figure 53: Geodesic structure cut at arbitrary plane: (a) view from the top; (b) perspective; (c) pieces to be produced.*

The current development of the parametric definition identifies the number of different hubs required for the dome (hubs of 5, 6 or 8 notches). This development, however, does not inform how many interconnecting parts are different in geometry, and in what way they are different. Knowing if only the pin position is different, but the overall geometry of the part is the same could be valuable. This is further discussed in Section 6. The parametric definition of hub type selection was confirmed.

## 5.2.2 Inflated surface

For the second application, the purpose is to produce a varying curvature surface where it may resemble a real-world structure. The boundary curve is created to resemble the shape of velodromes.

A quadrangular planar surface is created and discretized. Then, the produced mesh is modified through a mesh relaxation algorithm from the Grasshopper add-on Kangaroo (Piker 2017). Goals inserted in the solver are length of bars, boundary curve, and mesh volume. The mesh volume is the component that produces the inflated dome-like curvature to the surface. After this process, some smaller elements are observed clustered in four locations around the boundary curve of the surface. These correspond to the locations of the four vertices of the original quadrangular plane. On these locations, the mesh is edited to have one or two elements less. After those adjustments, the mesh is inserted into the already developed parametric definition. The notch geometry is slightly changed and scaled up, the hub and tubular dimensions are also scaled up. A second layer is also generated from an offset mesh. Figure 54a shows the final form, and Figure 54b shows a zoomed area where both layers can be observed and the connections are visible.



| a | b |
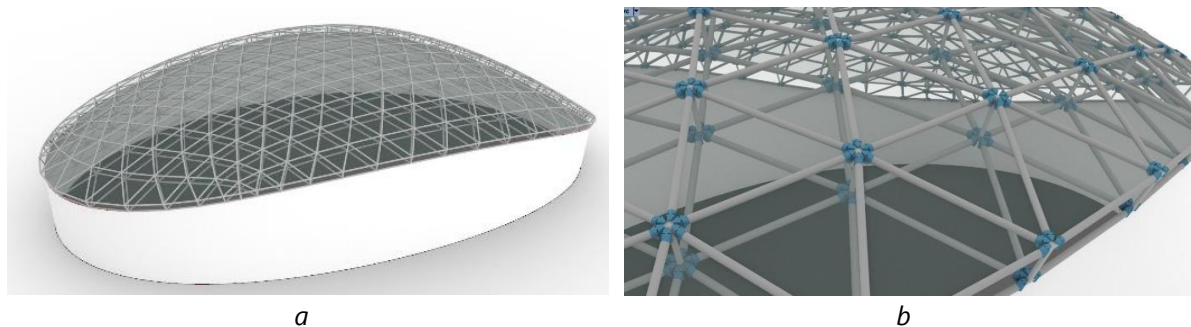
*Figure 54: Application of the system on a freeform surface: (a) global view; (b) local view.*

## 5.2.3 Wave-like surface

This application is meant to show the geometric capacity of the programmed cluster and validate the use of this system for unconventional surfaces. It is not the intent, in this application, to produce a stable structure. This surface resembles the shape of a breaking sea wave. The surface is constructed through a series of sectional curves. The mesh is generated with the triangulation of the quadrangular discretized surface. It takes a considerable amount

of computational effort to complete this application, and eventually, bugs are found in the resulting geometries. Recomputing the model solves this issue, however, it can take up to two hours. The final geometry is presented in Figure 55.

This application can provide insights of the quality of the programmed geometric parameters. This is discussed in Section 6.
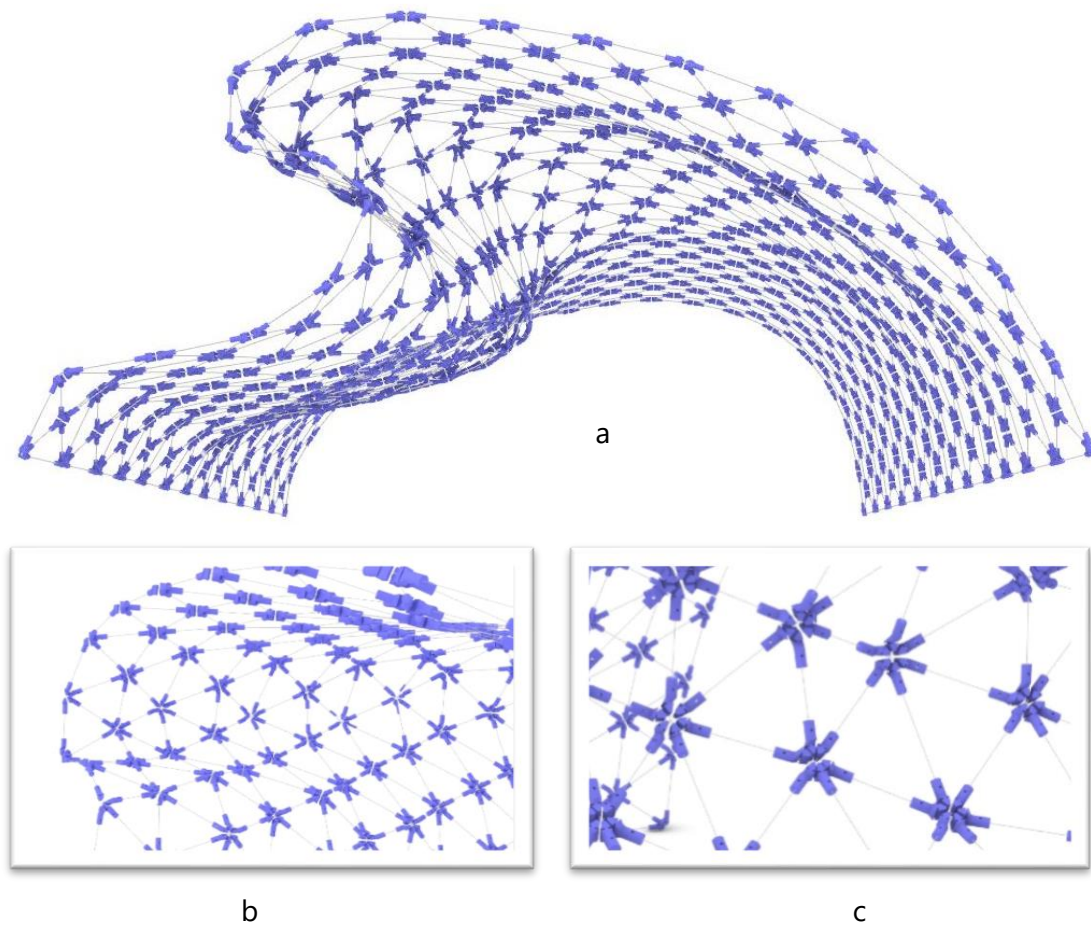


*Figure 55: Wave-like surface: (a) perspective view; (b and c) detailed views.*

# 6 Discussion

The present study developed a connection system for metallic reticulated structures. A solution was proposed for small scale applications where low cost and readily available materials were used. It was a constant concern to create a system that provided feasibility to gridshells with a complex surface and that provided scalability of the modeled concept. It was found that larger scales of this system are viable: higher strength plastics are available for 3d printing at elevated costs, but they are not prohibitive.

The amount of time required to print the interconnecting parts for the small-scale model was considered lengthy. Recent connection system developments present solutions where the entire connection is printed (Kassabian, Cranston, and Lee 2017; Van Der Linden 2015; N. Williams et al. 2015). The way these solutions found to print the least material possible was to apply topology optimization to the connection. The complete size of the connection, however, is still the same. As previously stated, the system in the present study is based on printing the least amount material possible; the time required for 3D printing production confirmed this need. The rapid development of new machines and materials that print faster with high quality does not indicate, so far, a considerable reduction in cost for those options.

Building a small-scale model was extremely relevant to raise questions on machine tolerance, best ways of directing pinholes, and other questions that, otherwise, would not have been brought up. The tolerances for the printing machine were easily applied to the computer model since the interconnecting parts geometries were expected to need fast changes. The available variable parameters were well suited. The tolerances for the bars, on the other hand, were not explored at the beginning of the program. Nevertheless, the solution was quickly implemented to adjust the size of each line that corresponded to the bars. These last-minute necessary changes tested the organization of the visual programming canvas. The organization of the workflow was found to be well reasoned. There was an effort to keep the variables, such as important points and lines, named and sets of components grouped. As the number of grouped components increased a short description of two phrases started being included for each group, which aided later changes. The data structure was also changed over the course of the program. The data organization proved to be essential, especially for large data sets, providing more efficient computation.

The tags for the 3D printed parts and bars was conceptually straight forward but it was not clear at first if the instructions and the logic would be intuitively followed by others. This was tested throughout several moments for the small-scale model. The instructions for the bars with different lengths were used by the technician in the mechanical laboratory, the material was delivered already tagged. This step was proved to be well executed. The files for 3D printing proved to be organized as well, although the letters used to indicate each color for each batch should have been clearer. Perhaps it would be practical to print a thin layer of material along with the batch to identify which files had been printed and which had not. The only way to verify the already printed batches was to open each file and to check the tags on the pieces.

Later, the assembly of the model was conducted by other team members, and some valuable feedback was provided. The tags were understood, and the assembly was conducted smoothly, however, some minor obstacles were noted. The printed pieces were being connected first to the hub, and then to the bars. This created confusion as to which notches had a printed piece and which should be left empty. Following, all bars and pieces were connected, except for the last one. The last bar did not fit smoothly in the last printed piece; the team had to take the printed pieces from the hub, connect the piece to the bar, and only then reconnect it to the hub. This provides extremely important insight for the assembly sequence. The pieces should be first connected to all the bars, only then should the bars be connected to the hubs. Furthermore, the last bar to be positioned should be the one with the smallest incidence angles (the area with the largest radius of curvature).

Positioning the pieces in the bars prior to the hubs, however, raises another obstacle: the tag location. The printed pieces were tagged on the circular face that is hidden inside the bar once the printed piece is connected to the bar. The tags are, thus, are changed to be located on the upper face of the printed piece, as shown in Figure 56. Now, the orientation of the piece is given by the face with the tag, which should be faced upwards, or towards the outer side of the surface.

*Figure 56: Modification of tag for the interconnecting part.*

It was also found that 3D text tags for the printed pieces still requires improvement. For now, the programmed description takes the boundary curve of each number, only then it is extruded and closed into a solid.

Another modification to be implemented is to indicate there are is an empty notch adjacent to that interconnecting part. The intent is not to tag the hubs, since they are standardized throughout the structure, or only a few varieties may occur.

The materials of the built physical model were chosen without prior dimensioning since there were limited resources and limited readily available options. The common sense that guided the choice of sections and materials were consistent with the size and resistance of the printed PLA parts. This is inferred from the tensile test results of the connection presented in Section 5.1. An initial hypothesis is that the PLA would fail before the metallic components reached yield strength. Figure 51c and Figure 51d show otherwise: the screw and the tube were deformed.

The numbered tags were easily followed by the assembly team. Nevertheless, a further discussion on larger scale models is necessary. The numbers can increase largely, and may it not be practical to build. Further questions would be raised for a larger scale project, such as the order in which to stack elements in a pile so later it is in the construction order, which is mostly a logistics problem, but the element tags should be practical for all parties involved. QR codes and augmented reality are tools that can help the feasibility of larger and more complex structures.

The computer modeling applications presented in Section 5.2 provided several insights. First, it was noted that the interconnecting parts were generated correctly with different surfaces

and meshes. However, it is clear that the parametric definition was not developed with a focus on computational efficiency, but rather on the creative process of the connection system. Once parameters are well defined, further development of the node would require computational efficiency. Furthermore, a large number of adjustments for scale can be reduced with causal relations between the size of the bar elements and the connections. The extension vector from Section 4.13, for instance, could be calculated from model parameters. This extension vector amplitude could be set to follow a formulation that takes into account materials used and size of the tubular section of the grid elements, providing required resistance.

The application of the geodesic dome provided an example of a mesh that produces many parts with equal geometry. The project could benefit from different manufacturing procedures, such as using several standardized molds for casting. This line of work would require additional programming steps for the automation of production of such molds. These extended perceptions of the structural system leave room for improvement, which is included in Section 7.1, about future works.

# 7  Conclusion

A new connection system for gridshells with complex surfaces was proposed. The system can be assembled, disassembled, and reused. It is composed of tubular bars, a standardized hub, and interconnecting parts. A parametric model was successfully implemented to generate the geometry of interconnecting parts, and it applies to a variety of meshes. Furthermore, the concept created through a physical model was proven.

The geodesic dome application verified the correct selection of hub types by the piece of the program. The inflated mesh application proved the importance of adjusting parameters to accelerate the scaling of the model. The wave-like surface exemplified applicability to high surface curvature variability, showing the robustness of the parametric definition. The brief structural analysis of the physical model provided the exploration of a stable shape before production of model elements. Moreover, the assembly of the model provided feedback on the concept of the connection system and construction sequence.

The scalability of the developed solution is feasible, and further studies (section 7.1) may prove this system promising to large scale production.

## 7.1 Future Work

The importance of detailed in structural analysis software is required to proper sizing of the system; however, it is not in the scope of this study. It would be necessary to define different force combinations and moments to understand in detail how the hub, 3D printed parts and bars would perform in different situations. Combinations with eccentricities of forces are also important. The article "Research on the Static and Hysteretic Behavior of a New Semi-Rigid Joint (BCP joint) for Single-Layer Reticulated Structures" (Ma et al. 2017) is an example of how the detailed study should be carried out on finite element software. Further studies with variation of parameters for the hub-3Dparts-bars can be conducted with the use of genetic algorithms and simplified structural analysis.

Further variations of the connection must also be explored, such as combinations of hubs for a double layered gridshell with diagonals. To identify geometric patterns and similarities between the geometries of interconnecting parts is a way to apply different fabrication methods. An example is to use the same wooden formwork produced with CNC milling machine for a composite material. The opposite may also be a challenging line of work: to set a maximum number of different geometries for interconnecting parts and provide the optimization or the exploration of mesh generation and hub positions.

Another future development would be the implementation of a more efficient and user-friendly tools for eventual distribution. This work would require including more choices for the user, such as different and variable bar cross-sections in the same structure.

# References

3DHUBS. 2019. "Knowledge Base." 2019. https://www.3dhubs.com/knowledge-base.

3DPrintingIndustry. 2017. "The Free Beginner's Guide." 2017. https://3dprintingindustry.com/3d-printing-basics-free-beginners-guide.

Addis, Bill. 2014. "Physical Modelling and Form Finding." In *Shell Structures for Architecture*, edited by Sigrid Adriaenssens, Philippe Block, Diederik Veenendaal, and Chris; Williams, 33–43. Routledge.

Adriaenssens, Sigrid, Mike Barnes, Richard Harris, and Chris; Williams. 2014. "Dynamic Relaxation." In *Shell Structures for Architecture*, edited by Sigrid Adriaenssens, Philippe Block, Diederik Veenendaal, and Chris; Williams, 89–101. Routledge.

Adriaenssens, Sigrid, Philippe Block, Diederik Veenendaal, and Chris; Williams. 2014. *Shell Structures for Architecture: Form Finding and Optimization*. London and New York: Routledge.

"Architecture+Fabrication: MakeTANK." 2018. 2018. https://theneueguild.com/portfolio-item/bsa-make-tank/.

ASTM Standard D 638 -02a. 2003. "Standard Test Method for Tensile Properties of Plastics." *ASTM D 638 -02a* 08: 46–58. https://doi.org/10.1520/D0638-14.1.

Asymptote. 2010. "Yas Marina and Hotel." 2010. https://www.asymptote.net/yas-slide-show.

Bechthold, Martin. 2008. *Innovative Surface Structures: Technologies and Applications*. Abingdon: Taylor & Francis.

Bisplinghoff, Raymond L. 1969. "Aeronautical Research: Hearings before the United States House Committee on Science and Astronautics, Subcommittee on Advanced Research and Technology, Ninety-First Congress, First Session."

Build With Hubs. 2017. "Geodesic Domes Made Simple." 2017. https://buildwithhubs.co.uk/.

Charest, Philippe, André Potvin, Claude Demers, and Sylvain Ménard. 2019. "Assessing the Complexity of Timber Gridshells in Architecture through Shape, Structure, and Material Classification." *BioResources* 14 (January): 1364–78. https://doi.org/10.15376/biores.14.1.1364-1378.

Dalbéra, Jean-Pierre. 2010. "La Pavillon Du Japon (Expo. Universelle de Hanovre 2000)." https://commons.wikimedia.org/wiki/File:La_pavillon_du_Japon_(Expo._universelle_de_H anovre_2000)_(4936016394).jpg.

Danhaive, Renaud Alexis, and Caitlin T Mueller. 2015. "Combining Parametric Modeling and Interactive Optimization for High-Performance and Creative Structural Design." In *IASS 2015: Future Visions*.

Deb, Kalyanmoy. 2001. *Multi-Objective Optimization Using Evolutionary Algorithms-Wiley*. Chichester: John Wiley & Sons.

Dimčić, Miloš. 2011. "Structural Optimization of Grid Shells Based on Genetic Algorithms." *Universität Stuttgart*. Stuttgart: ITKE.

Filabot. 2019. "Filabot." 2019. https://www.filabot.com/blogs/news/57233604-the-misleading-biodegradability-of-pla.

Fragmaq. 2017. "Fragmaq." 2017. https://www.fragmaq.com.br/blog/compostagem-industrial-como-funciona-e-e-praticada-no-brasil/.

Geometrica. n.d. "Geometrica." Accessed December 14, 2018. http://www.geometrica.com.

Gerasimov, D. V., A. V. Kashin, Y. V. Lunev, A. A. Morozov, V. S. Shmakova, and A. V.; Averin. 2018. "Glass Covering 'Glass Bark' of the Natural Park 'Zaryadye' in Moscow." *Journal of the International Association for Shell and Spatial Structures* 59 (3): 225–28. https://doi.org/https://doi.org/10.20898/j.iass.2018.197.021.

Goldberg, Dana. 2018. "History of 3D Printing." Autodesk. 2018. https://www.autodesk.com/redshift/history-of-3d-printing/.

Hassani, Vahid, Zubin Khabaz, Felix Raspall, Carlos Banon, and David W. Rosen. 2019. "Form-Finding and Structural Shape Optimization of the Metal 3D-Printed Multi-Branch Node with Complex Geometry." *Proceedings of CAD'19*, no. June: 24–28. https://doi.org/10.14733/cadconfP.2019.24-28.

Hernández, Elisa Lafuente, Olivier Baverel, and Christoph Gengnagel. 2013. "On the Design and Construction of Elastic Gridshells with Irregular Meshes," 161–74. https://doi.org/10.1260/0266-3511.28.3-4.161.

Jiang, Yang, Tomás Zegard, William F. Baker, and Glaucio H. Paulino. 2018. "Form-Finding of Grid-Shells Using the Ground Structure and Potential Energy Methods: A Comparative Study and Assessment." *Structural and Multidisciplinary Optimization* 57 (3): 1187–1211. https://doi.org/10.1007/s00158-017-1804-3.

Kalvo, Raul. 2013. "SUTD Library Pavilion." *Arch Daily*. https://en.wikipedia.org/wiki/File:SUTD_library_pavilion.jpg.

Kassabian, Paul, Graham Cranston, and Juhun Lee. 2017. "3D Metal Printing as Structure for Architectural and Sculptural Projects." In *FABRICATE: Rethinking Design and Construction*, edited by Achim Menges, Bob Sheil, Ruairi Glynn, and Marilena Skavara, 196–201. UCL Press.

Kato, S. 2014. "Guide to Buckling Load Evaluation of Metal Reticulated Roof Structures."

Khazaeli, Pouya. 2009. "Bamboo Structure." *Domus*. https://en.wikipedia.org/wiki/File:Bamboo_Structure.jpeg.

Labonnote, Nathalie, Anders Rønnquist, Bendik Manum, and Petra Rüther. 2016. "Additive Construction: State-of-the-Art, Challenges and Opportunities." *Automation in Construction* 72: 347–66. https://doi.org/10.1016/j.autcon.2016.08.026.

Linden, Lennert Van Der. 2015. "Innovative Joints for Gridshells." TU Delft.

Linkwitz, Klaus. 2014. "Force Density Method." In *Shell Structures for Architecture*, edited by Sigrid Adriaenssens, Philippe Block, Diederik Veenendaal, and Chris; Williams, 59–69. Routledge.

Lionpeloux. 2013. "Gridshell of Créteil, France, 2013." https://commons.wikimedia.org/wiki/File:Gridshell_of_Créteil,_France,_2013.jpg.

Liu, Yang, Helmut Pottmann, Johannes Wallner, Yong-Liang Yang, and Wenping Wang. 2006. "Geometric Modeling with Conical Meshes and Developable Surfaces." *ACM SIGGRAPH 2006 Papers on  - SIGGRAPH '06*, 681. https://doi.org/10.1145/1179352.1141941.

Ma, Huihuan, W. Wang, Zhonghao Zhang, and Feng Fan. 2017. "Research on the Static and Hysteretic Behavior of a New Semi-Rigid Joint (BCP Joint) for Single-Layer Reticulated Structures." *Journal of the International Association for Shell and Spatial Structures* 58 (2): 159–72. https://doi.org/10.20898/j.iass.2017.192.817.

Maiola, Carlos Henrique. 1999. "Análise Teórica e Experimental de Treliças Metálicas Espaciais Constituídas Por Barras Com Extremidades Estampadas." Escola de Engenharia de São Carlos da Universidade de São Paulo.

Menges, Achim, Bob Sheil, Ruairi Glynn, and Marilena Skavara. 2017. "Fabricate. Rethinking Design and Construction." In *Fabricate 2017*, 114–21. London: UCL Press. https://doi.org/10.14324/111.9781787350014.

Mesnil, Romain, Cyril Douthe, and Olivier Baverel. 2017. "Non-Standard Patterns for Gridshell Structures: Fabrication and Structural Optimization." *Journal of the International Association for Shell and Spatial Structures* 58 (4): 277–86. https://doi.org/10.20898/j.iass.2017.194.893.

Mesnil, Romain, Cyril Douthe, Olivier Baverel, and Bruno Léger. 2017. "Linear Buckling of Quadrangular and Kagome Gridshells: A Comparative Assessment." *Engineering Structures* 132: 337–48. https://doi.org/10.1016/j.engstruct.2016.11.039.

———. 2018. "Morphogenesis of Surfaces with Planar Lines of Curvature and Application to Architectural Design." *Automation in Construction* 95 (August): 129–41. https://doi.org/10.1016/j.autcon.2018.08.007.

Mesnil, Romain, Cyril Douthe, Christiane Richter, and Olivier Baverel. 2018. "Fabrication-Aware Shape Parametrisation for the Structural Optimisation of Shell Structures." *Engineering Structures* 176 (September): 569–84. https://doi.org/10.1016/j.engstruct.2018.09.026.

Mitchell, Melanie. 1998. *An Introduction to Genetic Algorithms*. Cambridge: MIT Press.

"MX3D." n.d. Accessed July 7, 2019. mx3d.com.

NeoArchaic. 2018. "MESH+." http://www.neoarchaic.net/mesh/.

Ochsendorf, John, and Philippe Block. 2014. "Exploring Shell Forms." In *Shell Structures for Architecture*, edited by Sigrid Adriaenssens, Philippe Block, Diederik Veenendaal, and Chris; Williams, 7–12. Routledge.

Oya, Takanori, Syun-ichi Takagi, Jun-ya Okazaki, and Shiro Kato. 2016. "Buckling Strength of Steel Tubular Members Related to Semi-Rigidity of Gusset-Plate Connection for Spatial Structures." In *IASS 2016: Spatial Structures in the 21st Century*.

Piker, Daniel. 2017. "Kangaroo." https://www.grasshopper3d.com/group/kangaroo.

Pottman, Helmut, Andreas Asperl, Michael Hofer, and Axel Kilian. 2007. *Architectural Geometry*. Edited by Daril Bentley. *Bentley Institute Press*. First Edit. Exton, Pennsylvania: Bentley Institute Press. www.bentley.com/books.

Pottmann, Helmut, Sigrid Brell-Cokcan, and Johannes Wallner. 2007. "Discrete Surfaces for Architectural Design." *Design*, 213–34.

Pottmann, Helmut, Michael Eigensatz, Amir Vaxman, and Johannes Wallner. 2015. "Architectural Geometry." *Computers and Graphics (Pergamon)* 47: 145–64. https://doi.org/10.1016/j.cag.2014.11.002.

Pottmann, Helmut, Yang Liu, Johannes Wallner, Alexander Bobenko, and Wenping Wang. 2007. "Geometry of Multi-Layer Freeform Structures for Architecture." *ACM Transactions on Graphics* 26 (3): 65. https://doi.org/10.1145/1276377.1276458.

Preisinger, Clemens. 2013. "Linking Structure and Parametric Geometry." *Archit Design*, no. 83: 110–13. http://www.karamba3d.com/.

RAF. 1943. "Vickers Wellington Mark X." https://www.iwm.org.uk/collections/item/object/205210367.

Richardson, James N., Sigrid Adriaenssens, Rajan Filomeno Coelho, and Philippe Bouillard. 2013. "Coupled Form-Finding and Grid Optimization Approach for Single Layer Grid Shells." *Engineering Structures* 52: 230–39. https://doi.org/10.1016/j.engstruct.2013.02.017.

———. 2014. "Discrete Topology Optimization." In *Shell Structures for Architecture*, edited by Sigrid Adriaenssens, Philippe Block, Diederik Veenendaal, and Chris; Williams, 171–79. Routledge.

Schlaich, Jörg. 2014. "On Architects and Engineers." In *Shell Structures for Architecture*, edited by Sigrid Adriaenssens, Philippe Block, Diederik Veenendaal, and Chris; Williams, viii–xi. Routledge.

Schober, Hans. 2015. *Transparent Shells: Form Topology Structure*. John Wiley & Sons.

Seifi, Hamed, Anooshe Rezaee Javan, Shanqing Xu, Yang Zhao, and Yi Min Xie. 2018. "Design

Optimization and Additive Manufacturing of Nodes in Gridshell Structures" 160 (June 2017): 161–70. https://doi.org/10.1016/j.engstruct.2018.01.036.

Shigeta, Yukino, Akiko Kobayashi, Ken'ichi Minowa, Toshiyuki Ogawa, and Shiro Kato. 2015. "Optimization of Shape and Member Stiffness Distributions for Single-Layer Reticulated Shells of Rectangular Plan." *Journal of the International Association for Shell and Spatial Structures* 56 (185): 173–86.

Sinha, Ankur, Pekka Korhonen, Jyrki Wallenius, and Kalyanmoy Deb. 2014. "An Interactive Evolutionary Multi-Objective Optimization Algorithm with a Limited Number of Decision Maker Calls." *European Journal of Operational Research* 233 (3): 674–88. https://doi.org/10.1016/j.ejor.2013.08.046.

Tayeb, Frédéric, Baptiste Lefevre, Olivier Baverel, Jean-François Caron, and Lionel du Peloux. 2015. "Design and Realisation of Composite Gridshell Structures." *Journal of the International Association for Shell and Spatial Structures* 56 (1): 49–59.

Taz. 2006. "The Bloedel Conservatory."

Tedeschi, Arturo. 2014. *AAD, Algorithms-Aided Design: Parametric Strategies Using Grasshopper*. Potenza: Le Penseur.

Tellier, Xavier, Olivier Baverel, Cyril Douthe, and Laurent Hauswirth. 2018. "Gridshells without Kink Angle between Beams and Cladding Panels." In *IASS 2018: Creativity in Structural Design*. Boston.

Warton, James, Heath May, and Rodovan Kovacevic. 2017. "Automated Design-to-Fabrication for Architectural Envelopes: A Stadium Skin Case Study." In *FABRICATE: Rethinking Design and Construction*, 36–43.

Williams, Chris; 2014. "The Multihalle and the British Museum." In *Shell Structures for Architecture*, edited by Sigrid Adriaenssens, Philippe Block, Diederik Veenendaal, and Chris; Williams, 239–44. Routledge.

———. 2017. "Decisions to Be Made in the Design and Analysis of Gridshell Structures." ThinkShell. 2017. https://www.youtube.com/watch?v=VPSw3dRE6xQ&t=3216s.

Williams, Nicholas, Daniel Prohasky, Jane Burry, Kristof Crolla, Martin Leary, Milan Brandt, Yi Min Xie, and Hamed Seifi. 2015. "Challenges of Scale Modelling Material Behaviour of

Additive-Manufactured Nodes." In *Design Modelling Symposium*, 45–51. Copenhagen. https://doi.org/10.1007/978-3-319-24208-8.

Winslow, Peter. 2014. "Multi-Criteria Gridshell Optimization." In *Shell Structures for Architecture*, edited by Sigrid Adriaenssens, Philippe Block, Diederik Veenendaal, and Chris; Williams, 181–93. Routledge.

Yang, Yong-Liang, Yi-Jun Yang, Helmut Pottmann, and Niloy J. Mitra. 2011. "Shape Space Exploration of Constrained Meshes." *ACM Transactions on Graphics* 30 (6): 11. https://doi.org/10.1145/2070781.2024158.

Zip Tie Domes. 2017. "Our Geodesic Dome Connector - How It Works!" 25/12. 2017. https://www.youtube.com/watch?v=v_NnY_yYwuc&t=3s.